Calculation and interpretation of cloud peak supersaturations at the Jungfraujoch

Master's Thesis

Faculty of Science

University of Bern

presented by

Emanuel Hammer

2011

Supervisor:

Prof. Dr. Urs Baltensperger
Laboratory of Atmospheric Chemistry, Paul Scherrer Institut

Co-Supervisors:

Dr. Ernest Weingartner
Dr. Nicolas Bukowiecki
Dr. Zsófia Jurányi
Dr. Martin Gysel
Aerosol Physics Group, Paul Scherrer Institut

Advisor:

Prof. Dr. Margit Schwikowski
Laboratory of Radiochemistry and Environmental Chemistry, Paul Scherrer Institut
and
Oeschger Centre for Climate Change Research

I bring fresh showers for the thirsting flowers
From the seas and the streams;
I bear light shade for the leaves when laid
In their noonday dreams.
From my wings are shaken the dews that waken
The sweet buds every one,
When rocked to rest on their Mother's breast,
As she dances about the sun.
I wield the flail of the lashing hail,
And whiten the green plains under;
And then again I dissolve it in rain,
And laugh as I pass in thunder.

by Percy Shelly

Contents

Summary

Aerosols play an important role in climate; however, climate models still suffer from large uncertainties. Aerosols influence radiative forcing directly through scattering and absorption of solar and infrared radiation in the atmosphere but also indirectly by forming clouds. The so-called cloud albedo effect was classified as low level of scientific understanding in IPCC (2007). Thus, further research in aerosol-cloud interaction is needed to improve climate models and to get better climate forecasts.

In summer 2010 a measuring campaign called CLACE2010 took place at the Jungfraujoch. The Jungfraujoch is situated in the Bernese Alps in Switzerland at 3580 m asl. The measurement site usually is in the undisturbed free troposphere except in summer where injections of air parcels from the planetary boundary layer are possible. Due to the quite high frequency of clouds, the Jungfraujoch offers a good opportunity to study the aerosol-cloud interaction.

Two inlets were installed to measure all cloud droplets and aerosols (total) and non-activated aerosols up to a size of 2 µm (interstitial). In the laboratory, two Scanning Mobility Particle Sizer (SMPS) were connected to both inlets to get aerosol size distributions. A cloud condensation nuclei counter (CCNC) was connected behind the total inlet to get total number concentration of activated aerosols with pre-defined supersaturations. Additionally, a fog monitor (FM), particle volume monitor (PVM) and a sonic anemometer were installed outside. From the FM measurements, cloud droplet size distributions were retrieved. The sonic anemometer was installed next to the FM to detect 3-dimensional wind velocities and wind directions within clouds. The PVM measured the liquid water content (LWC) within a cloud. This value helped to establish a stable cloud period criterion (70% of time LWC must be above 5 mg m^{-3}).

The goal of the thesis was to calculate ambient peak supersaturations within a cloud at the Jungfraujoch and to analyze which parameters influence supersaturations the most. The 17-month climatology of CCNC measurements at the Jungfraujoch (JURÁNYI ET AL., 2011 in press) delivered the activation diameter (D_{50}), where 50% of particles were activated, for several predefined supersaturations. Ambient D_{50} values were calculated via measured total number concentrations of activated CCNs with the FM or with the difference of the two SMPS connected to total and interstitial inlet, respectively. With a power fit function, where the x-axis is the supersaturation and the y-axis is D_{50}, ambient peak supersaturation (SS_p) could be calculated. It was found that during CLACE2010 SS_p showed a mean value of ~0.26% and a median value of ~0.17%. Calculating SS_p with 25th and 75th percentile of climatology of D_{50} values it can be concluded that the calculated SS_p is not that much dependent on how precise D_{50} has been measured. The difference (relative error of D_{50} = ±13% and of SS_p = ±10%) is smaller than expected and thus, a relationship with other parameters such as air temperature and w can be investigated for SS_p.

With this study it can be concluded that the aerosol hygroscopicity is not the major component determining SS_p. It was observed that a decrease in air temperature correlated with increasing SS_p up to -3.5°C, while a reverse trend occurred for higher temperatures. Furthermore, the updraft velocity (w) influenced in some cases SS_p as well, but this needs further investigations. By making a distinction between convective and advective clouds it was observed that in the former cloud type an increase in w resulted in higher SS_p. Wind direction also matters: clouds coming from south had generally lower SS_p (average SS_p = 0.1%) with a distinct lower variability compared to the clouds coming from north.

Zusammenfassung

Aerosole sind eine wichtige Komponente in den verschiedenen Klimamodellen. Noch immer weisen Klimamodelle eine hohe Unsicherheit auf. Die Energiebilanz wird durch Aerosole stark beeinflusst, indem sie die solare und infrarote Strahlung direkt in der Atmosphäre absorbieren und streuen. Indirekt wirken sie auf die Strahlung durch Wolkenformation, wobei der sogenannte Wolkenalbedo-Effekt eine grosse Rolle spielt. Dieser Effekt wurde im Bericht des IPCC (2007) als schlecht erforscht klassifiziert. Somit ist es von grosser Wichtigkeit, Forschung im Bereich der Aerosol-Wolken Interaktion zu fördern, um Klimamodelle zu verbessern und so bessere Klimavorhersagen zu erhalten.

Im Sommer 2010 fand auf dem Jungfraujoch die Messkampagne CLACE2010 statt. Das Jungfraujoch befindet sich auf einer Höhe von 3580 m.ü.M, in den Berner Alpen der Schweiz. Der Messstandort befindet sich meistens unbeeinflusst in der freien Troposphäre mit Ausnahme im Sommer, da können Luftmassen aus der planetaren Grenzschicht bis auf Höhen des Jungfraujochs steigen. Da das Jungfraujoch sich oft in den Wolken befindet, bietet dies eine gute Möglichkeit Aerosol-Wolken Interaktionen zu erforschen.

Zwei Einlässe wurden während der Messkampagne installiert um alle Aerosole einzufangen, aber auch um nur die interstitiellen (unaktivierten) messen zu können. Im Labor der Messstation Jungfraujoch wurden zwei SMPS jeweils an den beiden Einlässen angeschlossen, um die Aerosolgrössenverteilungen zu messen. Ein Wolkenkondensationkernzähler (CCNC) wurde an dem totalen Einlass angeschlossen, um die Anzahlkonzentration aktivierter Aerosole mit vordefinierter Übersättigung zu messen. Weiter wurde ein Fog Monitor (FM), ein particle volume monitor (PVM) und ein Sonic Anemometer draussen auf dem Jungfraujoch montiert. Vom FM erhofft man sich die Grössenverteilung von Wolkentröpfchen zu erhalten. Das Sonic Anemometer wurde nahe dem FM installiert, um die lokalen Windgegebenheiten in dreidimensionaler Richtung innerhalb einer Wolke zu messen. Das PVM mass den Wassergehalt (LWC) innerhalb einer Wolke. Dieser Wert fand Verwendung in der Etablierung eines Kriteriums für stabile Wolkenperioden (während 70% der Zeit muss der Wassergehalt über 5 mg m^{-3} sein).

Diese Masterarbeit hat zum Ziel, die Spitzenübersättigung innerhalb einer Wolke auf dem Jungfraujoch zu berechnen und den Einfluss weiterer Parameter auf diese Variable zu analysieren. Der CCNC führte zur totalen Anzahlkonzentration von aktivierten Aerosolen für verschiedene vordefinierte Übersättigungen. Aus diesen Messungen konnte der Aktivierungsdurchmesser D_{50}, wo 50% aller Partikel aktiviert werden, berechnet werden. Dies geschah durch die Rückwärtsintegration der gemessenen Aerosolgrössenverteilung. Mit derselben Methode wurden D_{50}-Werte berechnet: Durch die Messung der Anzahlkonzentration von Wolkentröpfchen durch einen FM oder durch die Differenz der beiden SMPS (totales SMPS minus interstitielles SMPS) konnte durch das Gegenüberstellen der berechneten D_{50}-Werte (y-Achse) von einem CCNC-Scan und den vordefinierten Übersättigungen (x-Achse) mittels einer Potenzialfunktion die Spitzenübersättigung berechnet werden. Es wurde beobachtet, dass während der CLACE2010-Kampagne die Spitzenübersättigungen einen Mittelwert von 0.26% und einen Median von 0.17% aufwiesen. Da die Spitzenübersättigungen durch D_{50}-Werte aus der CCNC-Klimatologie berechnet wurden und dabei das 25. und 75. Perzentil miteinbezogen wurde, konnte man erkennen, dass der Einfluss der Variabilität der gemessenen D_{50}-Werte auf Spitzenübersättigungen viel geringer ist als zuvor angenommen. Weitere Parameter wie Temperatur und Aufwindgeschwindigkeit zeigen einen grösseren Einfluss auf die Spitzenübersättigung.

Mit dieser Arbeit wurde also gezeigt, dass die Hygroskopizität für die Bestimmung der Spitzenübersättigungen nicht hauptsächlich masgebend ist. Es wurde beobachtet, dass bei ansteigender Temperatur die Spitzenübersättigungen zunahmen bis zu einer Temperatur von ca. -3.5°C. Für höhere Temperaturen wurde ein gegenläufiger Trend beobachtet. Weiter wurde ein Zusammenhang zwischen Aufwindgeschwindigkeiten und Spitzenübersättigungen für einige bestimmte Fälle beobachtet. Durch die Differenzierung zwischen konvektiven und advektiven Wolken wurde erkannt, dass der erstere Wolkentyp eine bessere Korrelation mit der Zunahme von Aufwindgeschwindigkeiten und Spitzenübersättigungen aufweist als der letztere Wolkentyp. Weiter wurde beobachtet, dass Wolken, welche vom Süden herkommen, eine konstantere Spitzenübersättigung aufweisen als Wolken, welche vom Norden herkommen. Die Spitzenübersättigung dieser Fälle befindet sich um Werte von 0.1%.

Abbreviations

a_w	water activity
CCN	cloud condensation nucleus/nuclei
CCNC	cloud condensation nuclei counter (measurement device)
CLACE2010	name of measuring campaign (Cloud and aerosol characterization experiment)
CPC	condensation particle counter (measurement device)
CWC	condensed water content
D_{50}	activation diameter where 50% of particles are activated
D_{crit}	critical particle diameter (is assumed as D_{50})
DMA	differential mobility analyzer (measurement device)
DOF	depth of field (part of fog monitor, where the laser beam measures the hydrometeors)
DPH	Dew Point Hygrometer (measurement device)
e	vapor pressure (partial pressure of vapor in air)
E	saturation vapor pressure
FM	Fog monitor (measurement device)
JFJ	Jungfraujoch (measurement location at 3580 m a.s.l.)
KLS	Kleine Scheidegg (measurement location at 2061 m a.s.l.)
LWC	liquid water content within a cloud
N_{tot}	total number concentration of aerosols
$N_{tot\text{-}int}$	difference of total minus interstitial aerosol number concentration measured by SMPS
OPC	Optical Particle Counter (measurement device)
PSA	particle surface area per volume (e.g. [cm^2cm^{-3}])
PVM	particle volume monitor (measurement device)
RH	relative humidity [%]
SMPS	scanning mobility particle sizer (measurement device)
SS	supersaturation
SS_{crit}	critical supersaturation
SS_p	ambient peak supersaturation
T_{air}	air temperature
T_d	dew point temperature

1. Introduction

The Greenhouse effect has become a primary focus of scientific and public interest in the last few years. Carbon dioxide (CO_2) is considered to be the most important greenhouse gas beside methane, halocarbons and other greenhouse gases in the earth's energy budget (IPCC, 2007). Beside the heating effect of these gases, the earth's radiation budget is also influenced by the presence of aerosols by direct and indirect effects.

The Intergovernmental Panel of Climate Change (IPCC) is a scientific body evaluating the climate properties in past and future to evaluate possible risks and impacts of climate change caused by natural and human activities. In an irregular period the IPCC publishes assessment reports based on peer reviewed scientific literature. The next report (Fifth Assessment Report) is expected to be released in 2013 with a new chapter on Clouds and Aerosols (pers. comm. T. Stocker). Aerosols play an important role in cloud formation and influence climate by cloud albedo effect (IPCC, 2007). Since a sufficient concentration of aerosols is always available in the atmosphere the homogeneous nucleation of water droplets never occurs in nature. Thus, some aerosols act as cloud condensation nuclei (CCN) in the process of heterogeneous nucleation. As an air parcel, containing aerosols, is lifted surrounding air cools down and a supersaturated regime may occur. If a critical supersaturation is reached, CCN will grow to cloud droplets as long as the air parcel remains supersaturated. This activation process of CCN is of special interest to cloud evolution, which thus has an influence on cloud albedo effect. This thesis focuses on the interaction between aerosols and clouds, namely on the microphysical processes taking place during cloud formation.

1.1. Aerosols

"An aerosol is defined as a suspension of fine solid or liquid particles in a gas (…) that range in size from a few nanometers (nm) to tens of micrometers (µm) in diameter." (SEINFELD & PANDIS, 2006)

All types of aerosols are covered by this definition; even fog, cloud and rain droplets are described with it, but these are more hydrometeors as well as ice crystals and snowflakes. Aerosols exist in every air mass on Earth, and vary only in concentration and composition. The particles may either be anthropogenic or natural origin. Anthropogenic sources are e.g. car or plane exhaust, exhaust from industry, biomass burning, residential heating, from a barbeque or even from printers in offices. Aerosol particles from natural sources are e.g. sea salt, pollen, Saharan dust or volcanic ashes (BALTENSPERGER ET AL., to be submitted).

Commonly aerosols are described in the following four size classes based on the particle diameters (D_P) (SEINFELD & PANDIS, 2006):

Nucleation mode: $D_P < 10$ nm

Aitken mode (ultrafine mode): 10 nm $< D_P <$ 100 nm

Accumulation mode: 0.1 µm $< D_P <$ 2.5 µm

Coarse mode: $D_P > 2.5$ µm

Hydrometeors (or cloud droplets) are commonly within the coarse mode while car exhaust lies within the Aitken and accumulation mode. The size range of cloud droplets is usually

within 5 to 20 µm depending on location (marine cumulus clouds have larger droplets than continental cumulus clouds) (WALLACE & HOBBS, 2006). The nucleation mode is reserved for particles which have freshly nucleated from gas molecules.

1.2. Aerosols and Climate

Aerosols play an important role in climate; however, climate models still suffer from large uncertainties. Aerosols influence radiative forcing directly through scattering and absorption of solar and infrared radiation in the atmosphere. Three major effects are described in IPCC (2007) by which the atmosphere is influenced by aerosol particles: the direct effect, the indirect effect and the semi-direct effect. In Fig. 1.1, uncertainties are depicted from at least two effects. The black bars show the standard deviation from each part within recent climate models. It can be seen that the highest uncertainty in radiative forcing arises from the component of total aerosols which includes the direct and indirect effect.

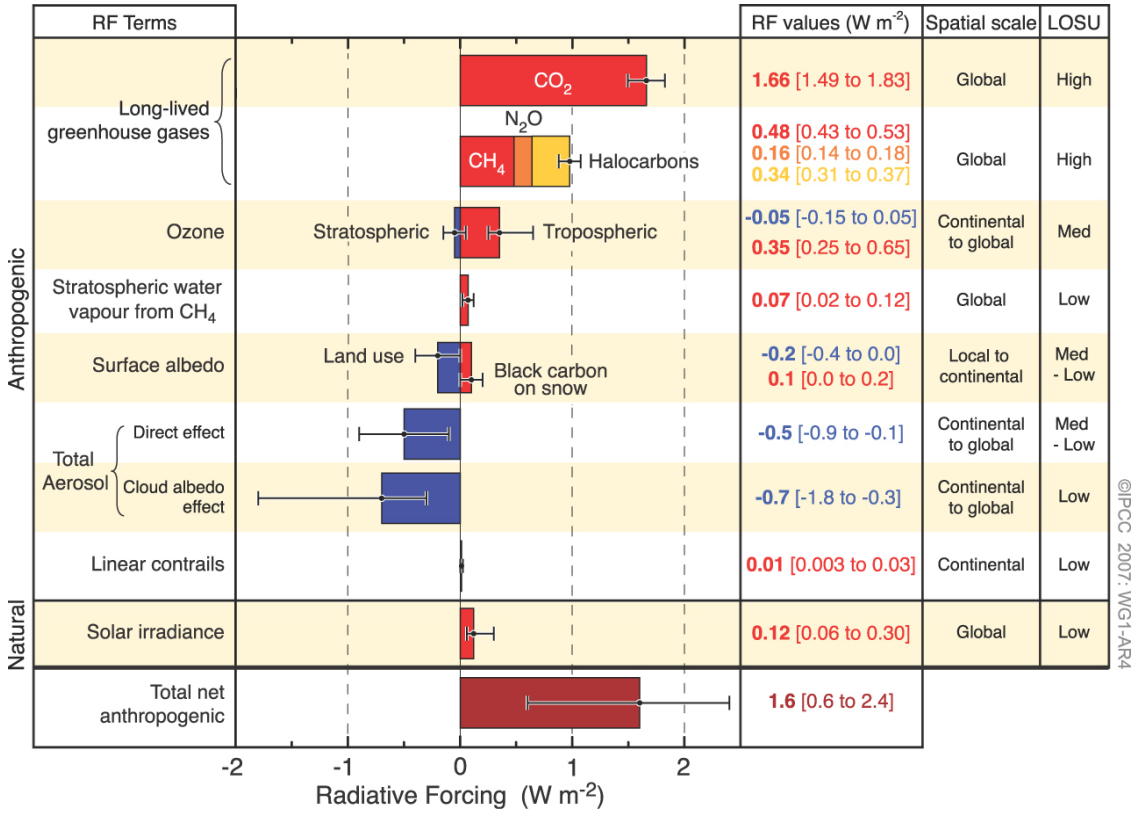

Fig. 1.1: Principal components of radiative forcing of climate change. The thin black line attached to each colored bar represents the range of uncertainty for the respective value. RF values show the influence on radiative forcing in Wm^{-2} with their geographical extent and the level of scientific understanding (LOSU). Volcanic aerosols are not considered due to their episodic appearance. (IPCC, 2007)

1.2.1. Direct effect

The direct effect is a mechanism, which describes the process of scattering and absorption of shortwave and longwave radiation by aerosol particles (depending on their composition), thus altering the Earth's radiative balance (see Fig. 1.2). Back-scattered light is directed back to space and cannot reach Earth's surface. This can be seen as a shielding process against sunlight radiation, similar to an umbrella. The scattering efficiency of an aerosol depends on its number concentration, angle of the sun to the particles, the optical properties of the particles and particle size (SEINFELD & PANDIS, 2006). If the aerosols are dark, solar radiation will be absorbed and, depending on the height of the aerosols in the atmosphere, a positive

feedback mechanism arises and results in a heating up the surrounding air. This positive forcing can be amplified if absorption of solar radiation by black carbon (BC) occurs within cloud particles or coated BC particle (CHYLEK ET AL., 1996).

The magnitude of the radiative forcing (expressed in Watts per square meters of surface) depends on the reflectivity of the underlying surface. The reflectivity of a surface, also called albedo, is characterized by the fraction of radiation that is reflected. A surface with a high albedo, e.g. a snowfield, will not absorb as much radiation as a dark surface, e.g. the ocean (SEINFELD & PANDIS, 2006). The net effect of the global aerosol is cooling with a negative radiative forcing of -0.5 Wm^{-2} (-0.9 to -0.1 Wm^{-2}) (IPCC, 2007).

1.2.2. Indirect effects

The indirect effect is the mechanism where aerosols indirectly influence the radiative forcing by altering the microphysical properties of the clouds. Through the uptake of water at high relative humidities (RH), aerosol particles are able to act as cloud condensation nuclei (CCN) or ice nuclei (IN) and thus are responsible for formation of cloud droplets. The effectiveness of an aerosol particle as a CCN depends on the size, chemical composition, mixing state and ambient environment (PENNER ET AL., 2001). When aerosols grow into cloud droplets, the amount of incoming radiation that is rejected increases dramatically, since the surface area of the particle is increased as well. The resulting cloud has a high albedo, up to 0.9 depending on their liquid water content (LATHAM ET AL., 2008), and will thus reflect about 90% of the visible light (SEINFELD & PANDIS, 2006).

Anthropogenic alteration of CCN number concentration modifies the cloud properties and thus affects climate. The amount of particles that are present in the atmosphere can, e.g., change the precipitation rate of a cloud.

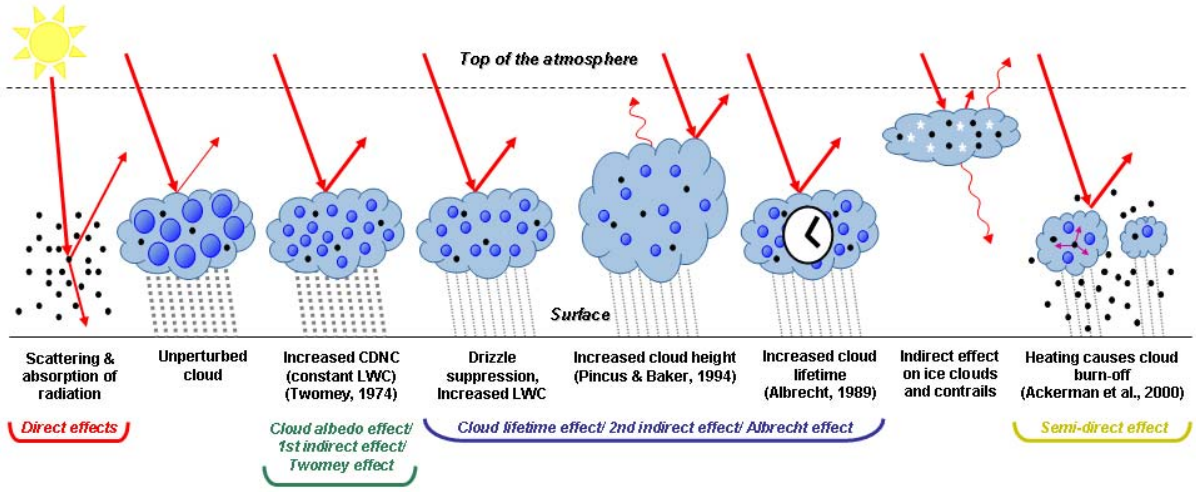

Fig. 1.2: Schematic diagram showing the various radiative mechanisms associated with cloud effects that have been identified as significant in relation to aerosols (modified from Haywood and Boucher (2000)). The small black dots represent aerosol particles, the larger blue circles cloud droplets. Straight red lines represent the incident and rejected solar radiation, and wavy red lines represent terrestrial radiation. The filled blue circles are cloud droplets and the white stars represent the ice crystals. CDNC stands for cloud droplet number concentration. The purple lines represent the heating from aerosol absorption within the cloud. The unperturbed cloud contains larger cloud drops as only natural aerosols are available as cloud condensation nuclei, while the perturbed cloud contains a greater number of smaller cloud drops as both natural and anthropogenic aerosols are available as cloud condensation nuclei (CCN). The vertical grey dashes represent rainfall, and LWC refers to the liquid water content. Modified from Cozic (2007), published in IPCC (2007)

1st indirect effect: Cloud albedo or Twomey effect

The first indirect effect describes the influence of the aerosol number concentration on cloud droplets (see Fig. 1.2). It is assumed that liquid water content (LWC) stays constant. With higher CCN number concentration, the available water is distributed over a larger surface and the reflectivity of solar radiation, termed cloud albedo, increases. Thus, more but smaller droplets are formed in warm clouds (TWOMEY, 1977). The 1st indirect effect results in an overall cooling of the atmosphere.

In total, a cooling effect from anthropogenic aerosols from the indirect cloud albedo effect of -0.7 Wm^{-2} (-1.8 to -0.3 Wm^{-2}) is expected (see Fig. 1.1).

2nd indirect effect: Cloud lifetime effect

For the 2nd indirect effect the LWC is assumed to be variable. A certain droplet size is required for a cloud droplet to grow to a rain droplet. This means if the particle size distribution is changed to smaller cloud droplets, precipitation is reduced (see Fig. 1.2). This inhibition of droplet growth leads to long-living clouds (ALBRECHT, 1989). Thus, the 2nd indirect effect contributes to a cooling of the atmosphere as well.

1.2.3. Semi-direct effect

The semi-direct effect describes the absorption of shortwave radiation by aerosols (such as soot particles). This effect depends on chemical composition and on the diameter of the particles. If particles absorb solar radiation, they heat up the surrounding atmosphere and thus alter relative humidity and stability of the atmosphere, while cloud formation and lifetime are influenced (IPCC, 2007). If the particles are within a cloud droplet and thereby absorb solar radiation, the increase of temperature can evaporate cloud droplets and reduce the cloud thickness (see Fig. 1.2). The reduced cloud thickness leads to a warming of the earth surface and to a warming in the atmosphere where particles absorb solar radiation. Nevertheless, more research is required to estimate the clear impact of semi-direct effect on the radiative forcing and thus to reduce the large uncertainties in the knowledge of Earth's atmosphere.

1.3. Jungfraujoch research station and CLACE campaigns

The International Foundation High Altitude Research Stations Jungfraujoch and Gornergrat provide the research station Jungfraujoch. The Foundation is dedicated to provide the infrastructure and support for scientific research of international significance. No research is carried out by the Foundation itself.

1.3.1. Jungfraujoch site

The high-alpine research station (46°32'N, 7°59'E) is located at 3580 m asl in the Bernese Alps on a crest between the two mountains Mönch (4099 m asl) and Jungfrau (4158 m asl). The station is easy accessible by train throughout the year. Local emissions are very low, since all heating is electrical and waste is shipped back to the valley. The special situation offers the opportunity to monitor background concentrations within the free troposphere. Meteorological data (wind speed and direction, temperature, humidity, pressure, radiation, etc.) are available from the automatic meteorological station of the Swiss meteorological institute (MeteoSwiss) located in the Sphinx observatory at Jungfraujoch (see Fig. 1.3). Due to the local topography the wind is channeled from NW to SE or contrariwise and the NW wind prevails 70-80% of the year (COZIC, 2007). The research station is within clouds about

40% of the time, thus it is a convenient location for studying microphysical cloud processes (BALTENSPERGER ET AL., 1998; SCHWIKOWSKI ET AL., 1995)

Fig. 1.3: Sphinx laboratory at Jungfraujoch with view to South-East. (COZIC, 2007)

1.3.2. CLACE campaigns

In the last years several measurement campaigns focusing on aerosol-cloud interaction studies have been conducted at the Jungfraujoch site. These campaigns called CLACE (Cloud and Aerosol Characterization Experiment) have been performed during summer and winter within international collaborations (Germany, United Kingdom, Hungary and Denmark). During these campaigns parameters like carbonaceous aerosol fraction, cloud droplet size distribution, liquid water content, interstitial aerosol size distribution, etc., were measured additionally to the continuous measurements at Jungfraujoch station. The goals of these intensive campaigns are (COZIC, 2007):

- A full physical, chemical, and optical characterization of the aerosol at the Jungfraujoch in order to better quantify the direct aerosol effect.
- An investigation of the interaction of aerosol particles with clouds, for a better quantification of the aerosol indirect effect.

The data discussed in this master's thesis were collected within the CLACE2010 campaign (June-August 2010). During this campaign an interstitial inlet was installed additionally to the heated total inlet (see section 3.1). More details about the deployed instruments behind these inlets and the instruments outside can be found in the methods section 3.1.

1.4. Motivation

Uncertainties from the contribution to the radiative forcing by aerosols are much higher than for the greenhouse gases (IPCC, 2007). With improving knowledge about the indirect aerosol effect, more reliable climate projections or even meteorological forecast can be provided. The interaction between aerosols and clouds is strongly dependent on the ambient supersaturation of water vapor. To date no measurement device is available that measures the actual supersaturation within a cloud. Thus, measurements discussed within this master thesis focus on CCNs determined by an artificial supersaturation produced in a CCN counter (CCNC), and CCNs produced by the actual supersaturation (ambient peak supersaturation) in a real cloud that is provided by a fog monitor (FM-100, Droplet Measurement System). In addition to the CCNC and the FM, a scanning mobility particle sizer (SMPS) will measure particle size

distributions. During this measurement campaign, the SMPS measured the total and interstitial aerosols simultaneously; this leads to high time resolutions (in earlier campaigns, only one SMPS has been used connected to a switching inlet). For the presence of a liquid cloud, the difference in the instrument responses is considered representative of the aerosol that is incorporated into the cloud phase. The relative difference of the size spectra gives information on the critical dry diameter. The overall aim of this master's thesis was to study the aerosol-cloud interactions within the CLACE2010 campaign performed at the Jungfraujoch.

2. Theory

2.1. Evaporation and condensation of water vapor

Water vapor is a minor constituent of the atmosphere (volume mixing ratio < 0.03) but still plays a crucial role in weather and climate processes as described in chapter before. Considering a transparent bottle partly filled with liquid water gives an adequate experiment to show the processes of condensation and evaporation. Water molecules in the closed bottle are moving randomly in all directions. During this movement some molecules gain enough speed (kinetic energy) due to collision with neighboring molecules, such that they can overcome the attraction in the liquid and will enter space above. This means the water molecule moved from the liquid to the gas phase. This process is called *evaporation*. The reverse mechanism, the transition from the gas to the liquid phase, is called *condensation*. With increasing amount of water molecules in the space above liquid the rate at which they return also increases. Hence, a dynamic equilibrium exists: the amount of liquid phase in the bottle remains constant as does the amount of water vapor above, although, there is a continuous exchange of water molecules between the two phases (ANDREWS, 2010).

The amount of water vapor over a flat surface at equilibrium with its surrounding is only a function of temperature. As temperature is increased the amount of water vapor increases as well. This is confirmed by the kinetic energy of water molecules in liquid: the greater the temperature, the greater the kinetic energy of water molecules in liquid phase. Thus, the chance of molecules escaping from the liquid phase is increased. Further, a relationship between evaporation and condensation rate exists: if the evaporation rate is increased the larger will be the amount of water vapor once the equilibrium is reached (NESSLER, 2004). A larger amount of water vapor compared to liquid leads to an increased condensation rate (see Fig. 2.1).

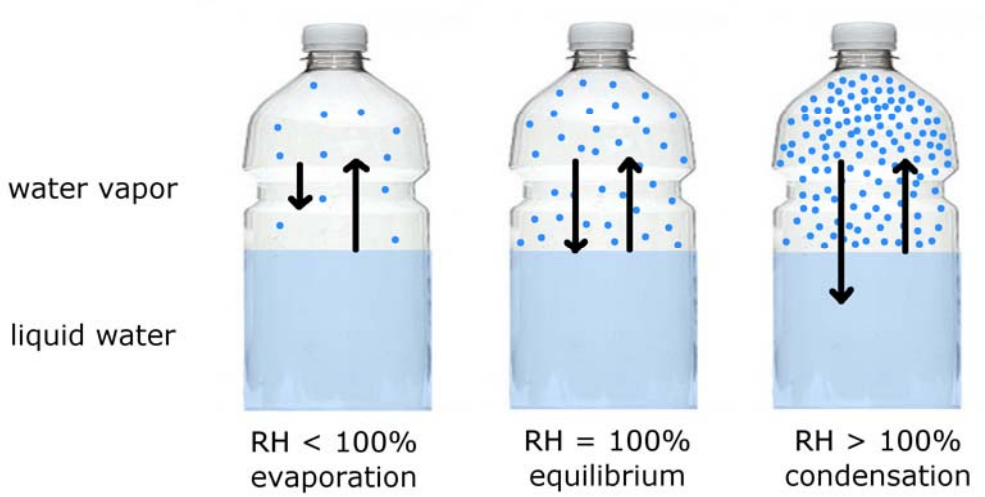

Fig. 2.1: Sketch of water vapor fluxes for RH < 100% (evaporation), RH = 100% (equilibrium) and RH > 100%. Downward arrows symbolize condensation rates and upward arrows symbolize evaporation rates. The intensity of its fluxes is given by the length of arrows.

The concentration of water vapor is often expressed as partial pressure of water vapor. Under these circumstances partial pressure of water vapor or also vapor pressure is denoted by the symbol *e*. When its concentration is equal to the equilibrium value (at phase transition), the corresponding vapor pressure is called saturation vapor pressure *E*. The Saturation vapor

pressure is defined for water vapor in the presence of air and in equilibrium with a flat surface of pure water. Another important measure of vapor pressure in air is given by relative humidity RH, defined by

$$RH = \frac{e}{E} \qquad \textbf{Equation 2.1}$$

RH is usually expressed in percentage (ANDREWS, 2010).

A physical relationship between rate of condensation/evaporation and *RH* is given. This cohesion is schematically shown in Fig. 2.1. Three cases can be distinguished (NESSLER, 2004):

- *RH* < 100% (subsaturation): The water vapor pressure *e* is smaller than the equilibrium value *E*, i.e., the rate of evaporation exceeds the rate of condensation → net evaporation
- *RH* = 100% (saturation): The water vapor pressure *e* equals the equilibrium value *E*, i.e., the rate of evaporation is equal to the rate of condensation → equilibrium
- *RH* > 100% (supersaturation): The water vapor pressure *e* is higher than the equilibrium value *E*, i.e., the rate of condensation exceeds the rate of evaporation → net condensation

2.2. Theory of Clausius-Clapeyron

The Clausius-Clapeyron equation describes how the saturated vapor pressure changes with changing temperature. The equation is named after Rudolf Clausius and Benoît Émile Clapeyron in 1834 (JENSEN, 2003). In Fig. 2.2 the parameterized Clausius-Clapeyron curve is depicted. At the different phase transitions, by considering a plane interface, vapor is saturated which means vapor is in equilibrium with the other phase. The Clausius-Clapeyron curve is given by

$$\frac{dp}{dT} = \frac{\partial S}{\partial V} = \frac{L}{T\partial V} \qquad \textbf{Equation 2.2}$$

where ∂S is the entropy gained as units of mass for the transition of water from liquid to vapor, L is the latent heat of vaporization per unit mass for the transition from liquid to vapor and ∂V is the increase of volume as unit mass as water changes from liquid to vapor. Actually, the specific volume V_v of the water vapor is much greater than that of the liquid; thus, $\partial V \approx V_V = 1/\rho_v = R_V T/p$ using the ideal gas law for water vapor. Here ρ_v is the vapor density and R_V is the specific gas constant for vapor. By using the ideal gas law, Clausius-Clapeyron equation can be written in the more convenient form

$$\frac{dp}{dT} = \frac{Lp}{R_v T^2} \qquad \textbf{Equation 2.3}$$

where *p* and *T* refer to the values at the phase transition. By these considerations pressure *p* and temperature *T* apply to water vapor on its own, but can also be applied to a volume of a mixing of vapor and surrounding air. In that case *p* has to be replaced by the partial pressure of water vapor *e*. At the phase transition the saturation vapor pressure *E* is present (ANDREWS, 2010).

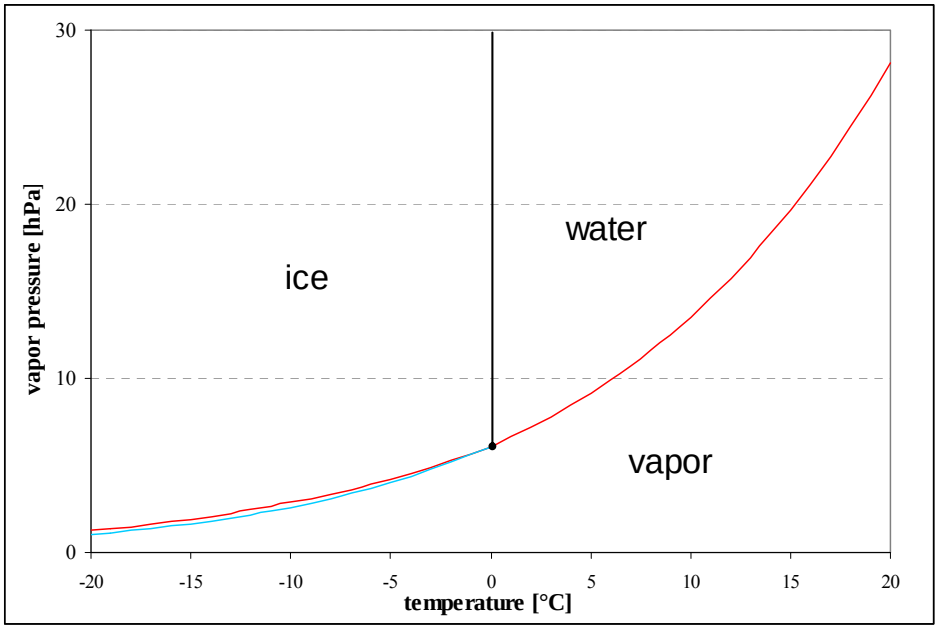

Fig. 2.2: Clausius-Clapeyron Curve with described phase transition between all three phases solid (ice), liquid (water) and gas (vapor). Triple point (p=6.1 hPa, T=273K) is shown where all the transition lines come together. The red line shows the saturation vapor pressure over water and the light blue line shows the saturation vapor pressure over ice. This is shown as example for the difference in dew point and freezing point temperature.

The dew point temperature T_d is the temperature of an air package to which the air must be cooled down at constant pressure, conserving its water vapor content, to get saturated. This means if the ambient air temperature is equal to the dew point temperature the following relation is given: $E(T_d) = e$.

In addition to the vapor-liquid phase transition, there are also solid-liquid and solid-vapor transitions. These three transition regimes cross one another at the triple point, which is at temperature $T = 273$ K and pressure $p = 6.1$ hPa as shown in Fig. 2.2. The phase transition line solid-vapor shows a small difference in comparison to the line of liquid-vapor: This difference is depicted in Fig. 2.2 with the two lines below 0°C. The blue line indicates the transition line between solid-vapor and the red line indicates the phase transition line in case the available water would still remain liquid below 0°C. The difference between these slopes is due to the difference in their specific volume V and latent heat as shown in Equation 2.3. Since $V_{vapor} >> V_{ice}$ and the two latent heat of ice-vapor and water-vapor are fairly similar, the two curves are quite close. However, the slope of the solid-liquid transition curve is very different. Here ∂V is small and negative as V_{liquid} is slightly smaller than V_{ice} but the latent heat is strongly positive, hence the solid-liquid transition has a large negative slope (WALLACE & HOBBS, 2006; ANDREWS, 2010).

Lowe and Ficke (1974) retrieved parameterization coefficients for the Clausius-Clapeyron curve from (good) laboratory results. The parameter coefficients are specified in Table 2.1 (SEINFELD & PANDIS, 2006). The range of validity is -50 to 50°C for water and -50 to 0°C for ice. These sixth order polynomials for both the ice and liquid water reference are expected to give errors of less than one percent for the entire meteorological range of interest.

Table 2.1: Parameterized Clausius-Clapeyron curve for saturation vapor pressure of water vapor over a flat pure water or ice surface

$E\ (hPa) = a_0 + a_1T + a_2T^2 + a_3T^3 + a_4T^4 + a_5T^5 + a_6T^5$ (T is in °C)	
water (-50 to +50°C)	ice (-50 to 0°C)
$a_0 = 6.107799961$	$a_0 = 6.109177956$
$a_1 = 4.436518521e^{-1}$	$a_1 = 5.034698970e^{-1}$
$a_2 = 1.428945805e^{-2}$	$a_2 = 1.886013408e^{-2}$
$a_3 = 2.650648471e^{-4}$	$a_3 = 4.176223716e^{-4}$
$a_4 = 3.031240396e^{-6}$	$a_4 = 5.824720280e^{-6}$
$a_5 = 2.034080948e^{-8}$	$a_5 = 4.838803174e^{-8}$
$a_6 = 6.136820929e^{-11}$	$a_6 = 1.838826904e^{-10}$

2.3. Activation of aerosol particles in warm clouds

Cloud droplets are formed within a supersaturated atmosphere with respect to liquid water. This means that relative humidity must exceed 100% to activate an aerosol particle and thus form a cloud droplet. The most common ways to produce supersaturated air is by air ascent. In this case air expands and adiabatically cools so that water vapor condenses on surrounding particles (*heterogeneous nucleation*) or spontaneously formation of liquid droplets without any nuclei (*homogeneous nucleation*). The process of homogeneous nucleation is the nucleation of vapor on embryos comprised of vapor molecules only, i.e. water vapor is surrounded by perfectly clean air – it has never been found in nature (SEINFELD & PANDIS, 2006; WALLACE & HOBBS 2006; MC FIGGANS ET AL., 2006).

In the previous sections only the case of a flat surface between liquid and vapor was considered. However, this case is not directly applicable to the formation of cloud droplets due to their spherical shape. The Köhler theory combines two effects which describe processes during the formation of a cloud droplet, namely the Raoult and the Kelvin effect.

2.3.1. Raoult's law

The Raoult effect describes the process of decreasing saturation vapor pressure when dissolving a solute in water. When solute molecules are added to an aqueous solution they act as a shield and decrease the evaporation rate of water molecules (KAMMERMANN, 2010). In Fig. 2.3 it is shown that the surface is partly covered by solute ions; water molecules can therefore not evaporate on the full surface. Thus, with decreasing concentration of water molecules, vapor pressure is decreased over the solution resulting in a lower evaporation rate.

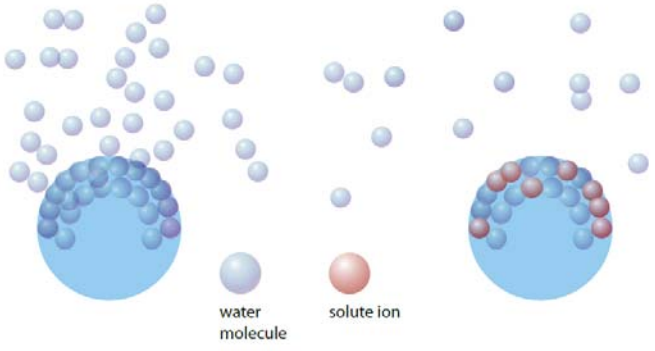

Fig. 2.3: The Raoult effect describes the decreased water vapor pressure in a solution droplet compared to a droplet of pure water. Solute ions are arranged also on the droplet surface that is exposed to evaporation. Water molecules are shielded by solute ions from evaporation, i.e. stay more in the droplet than without the solutes. (KAMMERMANN, 2010)

This issue in which water associates with various non-aqueous constituents is called water activity a_w and is defined as the vapor pressure of an aqueous solution $p_{solution}$ divided by that of pure water p_{H2O} at the same temperature:

$$a_w = \frac{p_{solution}}{p_{H_2O}} \qquad \textbf{Equation 2.4}$$

For ideal solutions the water activity can be calculated by (RAOULT, 1887)

$$a_w = \frac{n_w}{n_w + \sum n_i} \qquad \textbf{Equation 2.5}$$

where n_w is the number of molecules in moles and $\sum n_i$ is the sum of number of solute molecules in mol. By transforming Equation 2.5 one gets the Raoult's term in the Köhler equation (see Equation 2.9):

$$a_w = \exp\left(-\frac{6M_w \sum n_i}{\pi \rho_w D^3}\right) \qquad \textbf{Equation 2.6}$$

where ρ_w is density of water, D is the droplet diameter and M_w is the molar mass of water.

When applying Raoult's law to ambient aerosols, ideal solutions are often assumed. However, knowledge of the exact chemical compositions is necessary for calculations assuming non-ideality which are never available for ambient aerosols (JURÁNYI, 2010).

2.3.2. Kelvin formula

In addition to Raoult's law, the Kelvin formula describes the curvature effect and is referred to Gibbs-Thomson effect (ANDREWS, 2010). The curvature effect describes how the partial pressure of vapor e over a spherical droplet of diameter D_D in equilibrium state differs from saturation vapor pressure E, in the presence of surface tension. This means that small solution droplets, i.e. particles with a high surface curvature, exhibit a higher effective water vapor pressure since surface is larger in comparison to the volume. Thus, there is a higher saturation vapor pressure over curved surfaces in comparison to flat surfaces that come from higher surface tension of the droplets. Fig. 2.4 shows that in a smaller droplet, molecules are more exposed to the surface of the droplet and more likely evaporate (KAMMERMANN, 2010). Through the Gibbs-Thomson law one gets following equation for Kelvin's saturation S_{Kelvin}, which is included in the Köhler equation (ANDREWS, 2010):

$$S_{Kelvin} = \exp\left(\frac{4M_w \sigma_{sol}}{RT\rho_w D}\right) \qquad \textbf{Equation 2.7}$$

In comparison to Raoult's law, Kelvin's formula additionally depends on the surface tension of the solution σ_{sol}, the ideal gas constant R and the surrounding air temperature T.

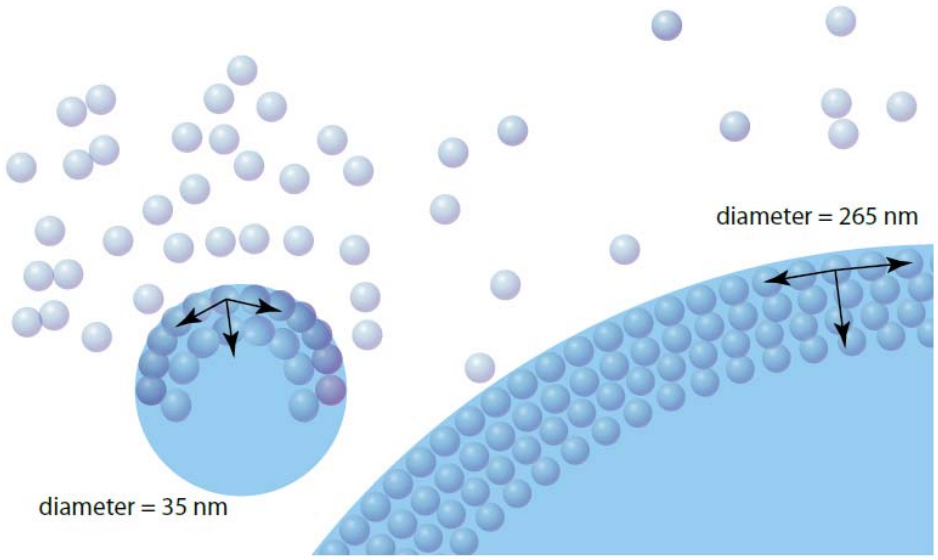

Fig. 2.4: A schematic illustration of the Kelvin effect. It describes the enhancement of the equilibrium vapor pressure over a curved surface compared to a flat liquid surface. It is shown that smaller droplets loose more likely water molecules to the gas phase than larger droplets. Black arrows indicate the approximate direction of attracting forces by neighboring molecules in the liquid. Note: The difference in equilibrium vapor pressure over pure water droplets of 35 and 265 nm in diameter is only 5%, i.e. the number of water molecules in the gas phase of the scheme does not resemble real conditions for illustrative purposes. (KAMMERMANN, 2010)

2.3.3. Köhler equation

The Köhler equation combines both the Raoult and Kelvin effect. It gives the relationship between equilibrium *RH* and the size of a solution droplet. In general, the equation can be used as follows:

$$RH = a_w \cdot S_{Kelvin} \qquad \textbf{Equation 2.8}$$

As already mentioned, the assumption of ideal solutions is a common way to approximate Köhler equation. Then it is written as:

$$RH = S = 100\% \frac{p_{H_2O}}{E_{H_2O}} = \exp\left(\frac{4M_w\sigma_{sol}}{RT\rho_w D} - \frac{6M_w \sum n_i}{\pi\rho_w D^3} \right) \qquad \textbf{Equation 2.9}$$

The maximum of this Köhler equation is called the critical supersaturation SS_{crit} $\left(SS = (S-1)\cdot 100\%\right)$ and is shown in Fig. 2.5. This Figure shows an example of the Köhler curve for a particle with a dry diameter D_{dry} of 50 nm. The diameter that belongs to SS_{crit} is called the critical diameter D_{crit}. For diameter $D < D_{crit}$ the droplet is in stable equilibrium (JURÁNYI, 2010). This means with an ambient *RH* of 100.3% and droplet diameter of 150nm condition *A* is present. A stable droplet of this kind is called a *haze* droplet. The condition is called stable as the addition of water in vapor phase to the droplet would increase its size but in order to keep this increased droplet size, a higher ambient saturation would be needed. However, the other point, *B*, will correspond to instability because a slight increase in droplet radius D_D will lead to condensation and therefore to a further increase in radius (ANDREWS, 2010). Thus, situations on the other side of the curve where $D > D_{crit}$ are instable. The process where an aerosol particle is growing to larger diameters than D_{crit}, is called the cloud droplet activation. A single aerosol particle, which is in surrounding air where supersaturation already

has reached SS_{crit}, will act as a cloud condensation nuclei (CCN). This means, when a CCN is activated, it takes up as much water as available in the surrounding (JURÁNYI, 2010).

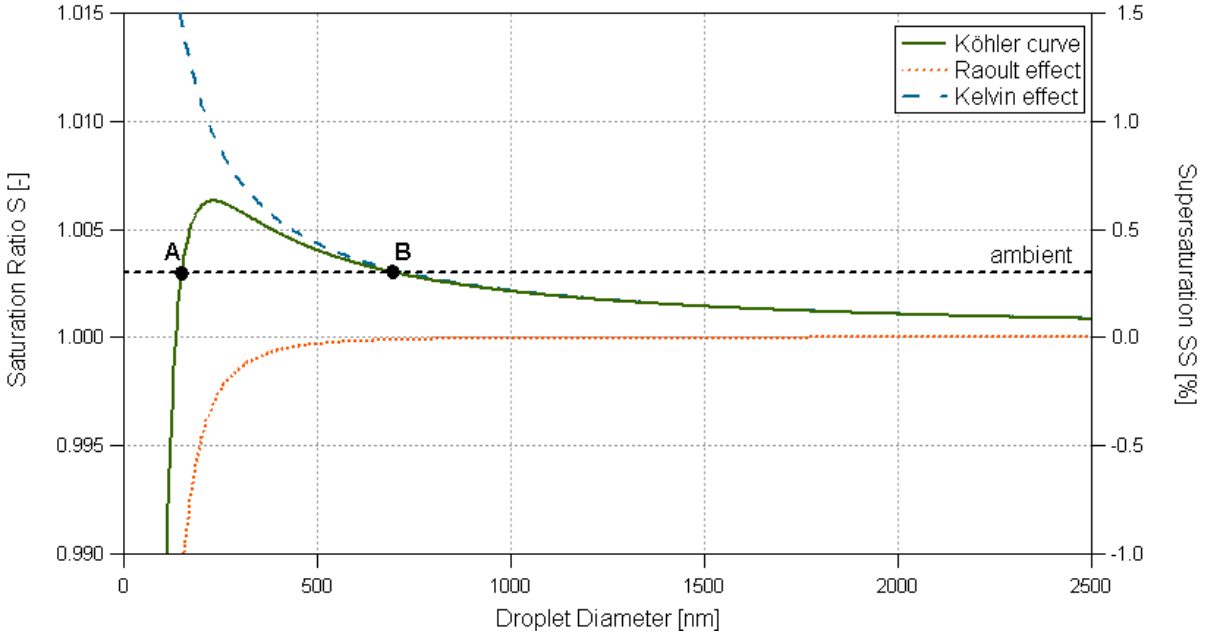

Fig. 2.5: Köhler curve (solid, green line) for the saturation ratio (S= e/E) and supersaturation (SS=(S-1)·100) for a spherical droplet of water containing solute as a function of droplet diameter D_D. The Kelvin effect is depicted with a blue dashed line and Raoult's effect is shown with orange dotted line. Dashed black line shows the ambient condition with A and B as example for stable and unstable conditions, respectively.

The value of a critical supersaturation SS_{crit} is always referred to one single aerosol particle. In ambient atmosphere or even within a Cloud Condensation Nuclei Counter (see section 3.1.2) just one supersaturation for a cloud droplet population is measured. This is the so-called peak supersaturation SS_p. It refers to the critical supersaturation where all measured, activated CCN could have reached SS_{crit}.

2.3.4. Activation diameter

The diameter where 50% of the particles are scavenged resulting by water is called activation diameter D_{50} and refers to the critical diameter D_{crit} from the Köhler equation (see section 2.3.3). Some studies have shown that D_{50} is a good value to approximate the theoretical value D_{crit} (CORRIGAN & NOVAKOV, 1999; HENNING, 2002; HARTZ ET AL., 2006, PRENNI ET AL, 2007). How D_{50} has been retrieved from the measurements analyzed in this thesis will be explained in section 3.2.

2.4. Droplet growth by updraft

A rising air parcel experiences adiabatic cooling and surrounding water vapor condenses onto cloud droplets due to supersaturated air. Thus, the updraft velocity (w) influences the influx of water vapor. Updraft velocity is proportional to parcel buoyancy, where the parcel buoyancy is a function of the temperature difference between the parcel and its environmental air. As water vapor is converted into liquid droplets it releases latent heat to the parcel, consequently increasing the temperature difference. This increased buoyancy will enhance the updraft and increase the water vapor influx (HOUZE, 1993). However, Rogers (1975) showed a quite clear connection between updraft velocity and supersaturation with a numerical parcel model.

3. Methods

3.1. Measurement devices

All analysis and results presented in chapters 4 and 5 are based on the measurements of aerosol and cloud droplet size distributions carried out on the Jungfraujoch. For the collection of aerosols an interstitial and a total inlet was installed at a fairly undisturbed place on the roof of the Sphinx laboratory at the Jungfraujoch. The interstitial inlet was installed for collecting particles smaller than 2 µm. It uses an aerodynamic size discriminator without heating (HENNING ET AL., 2002). Thus, all non-activated particles pass this inlet. The total inlet samples all particles smaller than 40 µm at wind speeds up to 20 ms^{-1} (WEINGARTNER ET AL., 1999). Hence, the total inlet samples cloud droplets and non-activated (interstitial) aerosols. The water surrounding the cloud droplets and aerosols is evaporated by heating up the total inlet to +20°C (HENNING ET AL., 2002). Behind the interstitial inlet a Scanning Mobility Particle Sizer (SMPS) system is installed to measure the size distribution of the interstitial aerosol. The total inlet carries the aerosols to a cloud condensation nuclei counter (CCNC) and to another SMPS system where the size distribution of all aerosols up to a size of 40 µm is measured.

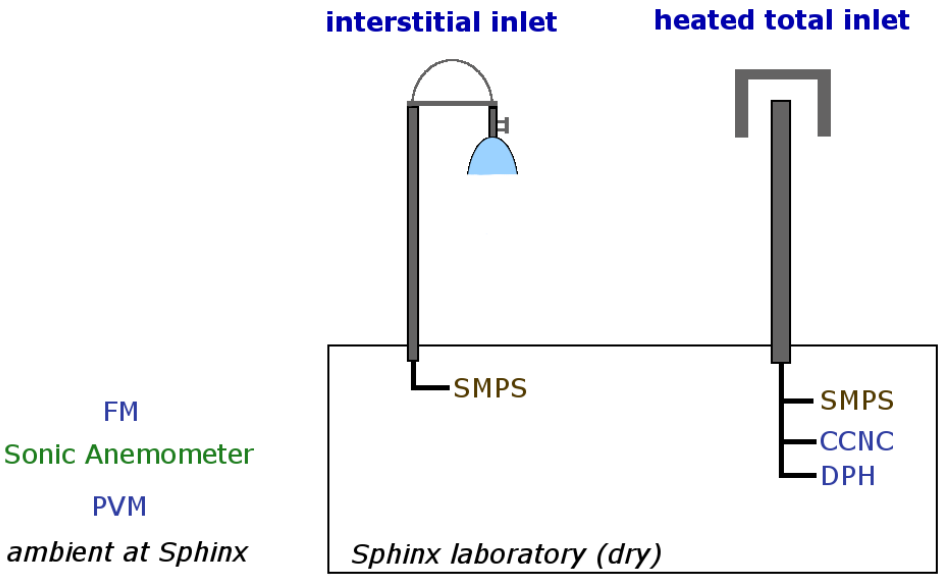

Fig. 3.1: Sketch of inside and outside measurement devices inside and outside at the Sphinx laboratory at the Jungfraujoch during CLACE2010 that were used in this work.

3.1.1. Aerosol size distributions

For the size resolved measurement of aerosol particles two commercially available SMPS systems (TSI Incorporated, USA) were installed, one behind the interstitial inlet and one behind the total inlet. Both systems were identical: they consisted of three major components: a bipolar charger, a Differential Mobility Analyzer (DMA) and a Condensation Particle Counter (CPC). Due to the fact that the mobility of charged particles in an electrical field is directly connected to their size, a bipolar charger with a krypton source (^{85}Kr) was installed (WEINGARTNER ET AL., 1999). The DMA can detect particles with certain mobility depending on their flow and voltage. After exiting the DMA, the selected particles enter a CPC, which measures the particle concentration. In the CPC butanol evaporates into the air stream and

saturates the flow, therefore, vapor condenses onto the airborne particles and this produces lager and easily detectable aerosol droplets (HENNING, 2002).

3.1.2. Artificial activation of aerosols

A Cloud Condensation Nuclei Counter (CCNC) was installed at the Jungfraujoch, which measured the number and size distribution of CCN's by self-defined supersaturations. This device is set up behind the total inlet.

The lowest supersaturation at which cloud condensation nuclei (CCN) can be measured in static diffusion chambers is greater than 0.2% due to insufficient time for droplet growth (NENES ET AL., 2001). This value is not low enough to match supersaturations found in stratus clouds. The CCNC device employs a robust method of precisely generating a supersaturation by maintaining a constant wall temperature gradient along the flow direction. The operating range of the CCNC with still reasonable values is between 0.13 and 3% supersaturation, although, the temperature gradient can be adjusted for much lower values. Due to a continuous flow a fast sampling is possible, which is suitable for airborne measurements (ROBERTS & NENES, 2005).

During the measurement campaign CLACE2010 the CCNC instrument was running with supersaturations from 0.07 to 1.18%.

3.1.3. Cloud droplet size distributions

The droplet size distribution of the cloud was measured at 12.5 Hz with an active high-speed FM-100 cloud particle spectrometer or fog monitor (Droplet Measurement Technologies, Boulder, CO, USA) so that the evolution of the cloud microphysics could be evaluated at a high time resolution. High rate measurements are important since many of the physical processes that determine cloud lifetime are highly inhomogeneous.

The fog monitor (FM) collects droplets in the size range 2-50 µm in up to 40 freely definable channels (EUGSTER ET AL., 2001). Data from the sonic anemometer and the FM were received asynchronously; using the open-source software *sonicreadHS* and the additional package *fm* by Werner Eugster (Grassland Sciences, ETH Zurich), the data was synchronized and merged. The FM device was provided by Institute for atmospheric and climate science at ETH Zurich (IAC) and the Sonic Anemometer was provided by Werner Eugster from the Grassland Sciences group at ETH Zurich.

From 14 June until 19 July the FM was running on a horizontal platform. A first look at the data revealed distinct values of liquid water content from the FM and the PVM. Taking data from the sonic anemometer into account it could be concluded that the vertical wind component has a large influence in addition to the horizontal wind component. Thus, it was suggested that the difference between the data is due to strong updraft velocities near the location of the FM. The platform at the FM was reinstalled on 19 July at an angle of 25° so that the cloud droplets could pass the inlet more undisturbed as can be seen in Fig. 3.2.

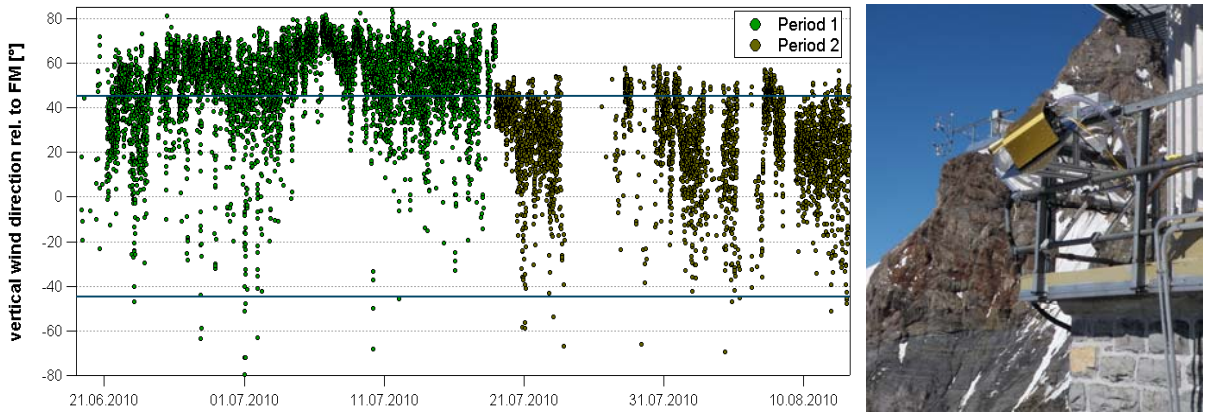

Fig. 3.2: Left: Vertical wind direction relative to the FM for periods, where FM was installed horizontally (green) and with a steepness angle of 25° (brown). Right: Measurement setup of fog monitor and sonic anemometer from July 19 to August 13.

Working principle of the FM-100

The FM consists of an inlet tube in front of the optical system. A regenerative pump pulls air through the optical system, where the flow rate is measured with a Pitot tube. Static pressure, differential pressure and ambient temperature are measured to determine air density and finally airflow is calculated in meters per second. Due to the fact that the pump was not weather resistant it had to be installed in a room protected from rain. A flexible tube of a length of 10 m connected the fog monitor and the pump.

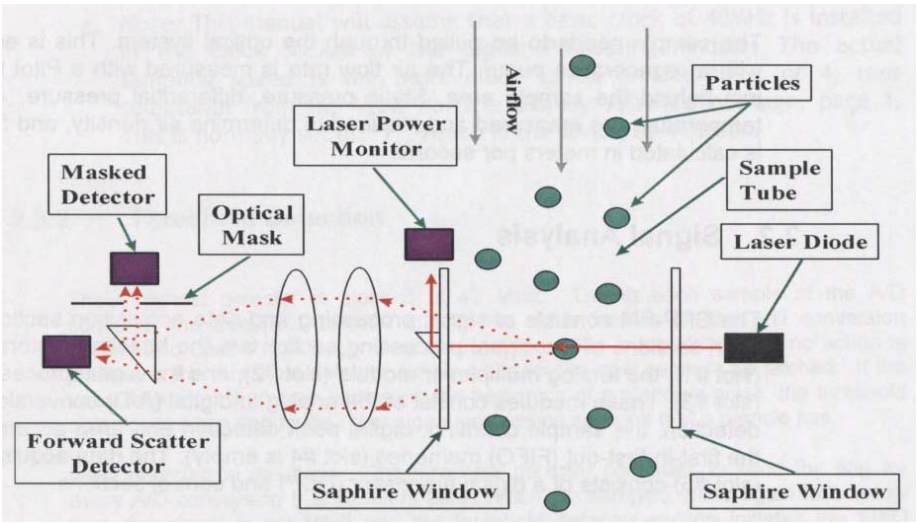

Fig. 3.3: Schematic view of the optical bench within a FM-100. Green dots are representing cloud droplets within a size range of 2-50µm. Laser diode is the source of the laser beam that will be detected from the laser power monitor and the classification of droplet size has been performed. Forward scatter detector is representing the signal detector which detects scattered light from particles passing through the beam (DMT Manual,1999).

When cloud droplets are present they are sucked into the inlet and pass an optical bench and the signal processing electronics (see Fig. 3.3). The optical bench collects light that is scattered from individual particles that pass through a laser beam, which has a Gaussian profile. Two photo detectors measure the collected light. The first sees 33% of the light and the second receives only light collected from particles that pass through the laser beam. The location, through which the particles pass is a small region near the center of focus called the *Depth of field* (DOF). These two detectors are referred to *Signal* and *Mask*, respectively.

Despite of the non-uniform intensity of the laser beam, either the peak value of scattered light or its total value can be used to characterize a particle's light scattering properties.

Calculating liquid water content

The liquid water content (LWC) quantifies the amount of water in cloud droplets and thus leads to the formation of cloud droplets. It is typically measured in units of mass per volume (e.g. g m^{-3}). With the Opticle Particle Counter (OPC) data measured by the FM the number of cloud droplets in each size bin can be retrieved. Applying the assumption that the volume of cloud nuclei is negligible, LWC can be calculated as:

$$LWC = \rho_w \cdot \frac{4}{3} \cdot \pi \cdot \frac{\sum_{i=1}^{i=m} N_i \cdot r_i^3}{SV} \qquad \textbf{Equation 3.1}$$

In Equation 3.1 m is the number of size bins; N_i and r_i are the number and radius of particles in each size bin i, respectively. Value ρ_w is the density of water surrounding the nuclei and is commonly assumed as 1.0 g cm^{-3}. SV is the sample volume calculated from the air flow rate through Pitot tube v_{FM}, sampling time t and sample area SA:

$$SV = v_{FM} \cdot t \cdot SA \qquad \textbf{Equation 3.2}$$

The sample area SA is defined by the length of DOF l_{DOF} multiplied by the effective beam diameter $d_{Beam,eff}$. This requires further explanation: as already mentioned the intensity of the laser beam is reduced its edges in comparison to its center due to the Gaussian profile of the light intensity. Thus, particles nearer the edges will appear undersized as they are less illuminated by the laser beam. These particles are rejected by comparing their measured transit times with a running average of previous particle transit times. If the transit time of the current particle is less than the average, the particle is rejected for sizing. The effective beam diameter finally is a fraction of the physical beam diameter. This fraction can be theoretically predicted as 62% of the physical beam diameter. However, it can also be directly calculated by the ratio of particles passing through the DOF. Thereby the ratio of velocity accepted particles (*gated strobes, GS*) and number of all particles passing through the DOF (*total strobes, TS)* has to be considered (DMT, 1999):

$$SA = l_{DOF} \cdot d_{beam,eff} \cdot \frac{GS}{TS} \qquad \textbf{Equation 3.3}$$

3.1.4. Wind field near the fog monitor

For the estimation of the average vertical wind speed component within the cloud and the wind field near the fog monitor, a HS ultrasonic anemometer (Gill Ltd., Solent, U.K.) was installed at an adequate distance of 1.7 m from the Sphinx facade and from the FM (see Fig. 3.4).

Fig. 3.4: Measurement setup from June 14 to July 19 of fog monitor and ultrasonic anemometer.

Taking both the wind direction and speed into account it can be determined whether the device setup was appropriate for the wind field and the cloud droplets could be sampled isokinetically (i.e. without impaction). This information is very important for the further analyses.

Before installing the platform of the FM, it had to be analyzed which are the main wind directions during the season of the campaign. In order to address this issue, data from SwissMetNet station at the Jungfraujoch provided by MeteoSwiss was used. In Fig. 3.5 one can see a wind rose of the months of June and July for 1990 to 2009. Thus, the FM inlet was pointed in the direction of 323° from June 14 to July 19. When the platform was inclined on July 19, the horizontal angle was set at 293° and the vertical angle (steepness) was -21°.

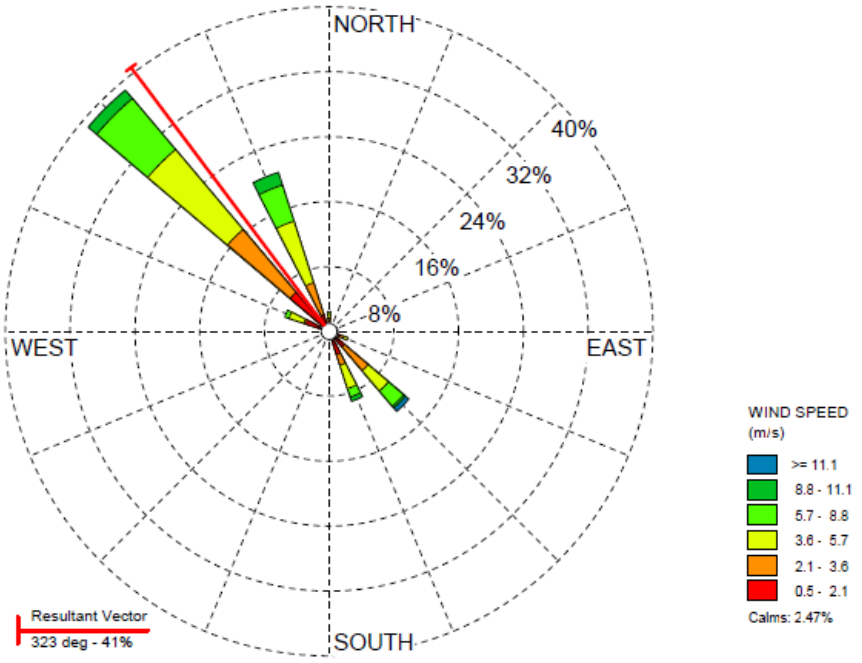

Fig. 3.5: Wind rose at Jungfraujoch during months of June and July from 1990 to 2009.

Another piece of information that is expected to be retrieved is the origin of the activation of aerosols. For this issue, data from a Windprofiler located at Kleine Scheidegg and operated by MeteoSwiss could help to determine the wind field further away from the location of measurement devices placed at Jungfraujoch.

3.1.5. Comparing data from FM-100 and PVM-100

For quality assurance, the FM-100 was compared to another instrument measuring cloud microphysical properties. A particle volume monitor (PVM-100, Gerber Scientific Instrument Inc.) was also provided during CLACE2010. This device measures the liquid water content (LWC) and the total particle surface area (PSA) of cloud droplets with a two-channel optical sensor. Due to the fact that the effective radius r_e is proportional to the ratio of LWC and PSA ($r_e \propto LWC/PSA$), this parameter is also provided by the PVM-100.

The value of r_e is a weighted radius of a size distribution and is a useful parameter for accessing the radiative effect of clouds (HANSEN & TRAVIS, 1974). Equation 3.4 shows the calculation from an arbitrary size distribution (HENNING ET AL., 2002), e.g. for data from the FM.

$$r_e = \frac{1}{2}\sum_{i=1}^{m} N_i D_i^{\,3} \Big/ \sum_{i=1}^{m} N_i D_i^{\,2} \qquad \textbf{Equation 3.4}$$

As the PVM-100 does not give a size distribution, r_e has to be calculated from LWC and PSA. As seen in Equation 3.1, LWC is calculated with the cubed radius. The value of the PSA is calculated with the squared radius as defined in Equation 3.5 (PVM, Gerber Scientific Instruments Inc.).

$$PSA = 4 \cdot \pi \sum_{i=1}^{m} r_i^{\,2} \cdot N_i \qquad \textbf{Equation 3.5}$$

Equation 3.1 divided by Equation 3.5 and multiplied with the factor $3/\rho$ leads to Equation 3.6. Thus, the value of r_e from PVM-100 data is defined as:

$$r_e = \frac{3 \cdot LWC}{\rho_w \cdot PSA} \qquad \textbf{Equation 3.6}$$

By assuming that the cloud measured by FM-100 is the same as the one analyzed by PVM-100, the LWC values can directly be compared.

3.1.6. CWC derived from temperature and dew point measurement

Applying the parameterization of the Clausius Clapeyron curve (Table 2.1), the saturation vapor pressure from ambient air (E_g) and the air heated up within the inlet ($E_{s,l,g}$) can be calculated. The denotations *s, l, g* stand for solid (ice), liquid (hydrometeors) and gas (vapor) phase respectively. The sketch in Fig. 3.1 shows that in ambient air water in both the liquid and gas phase (ice has been neglected due to the assumption that during CLACE2010 a negligible amount of mixed and iced clouds were present) was present, whereas in air reaching the DPH water is only present in the gas phase due to heating of the total inlet. Thus, the DPH measured a different saturation vapor pressure than would be given for ambient air. In the following Equation 3.7 only total condensed water content from ambient air $TWC(T_d)$ is considered and ambient water in vapor phase $VWC(T_{amb})$ has been subtracted:

$$CWC(T_d, T_{amb}) = TWC(T_d) - VWC(T_{amb}) \qquad \textbf{Equation 3.7}$$

TWC is the total water content from water in ambient air of all three phases (solid, liquid and gaseous). *VWC* is the vapor water content which describes the amount of water in vapor phase in the ambient air. From ideal gas law the following relationship can be achieved:

$$E_{l,g} \cdot V_{l,g} = \frac{m_{l,g}}{M_{H_2O}} \cdot R \cdot T_d \qquad \textbf{Equation 3.8}$$

and:

$$E_g \cdot V_g = \frac{m_g}{M_{H_2O}} \cdot R \cdot T_{amb} \qquad \textbf{Equation 3.9}$$

where E is the saturation vapor pressure, V the volume of air parcel, m the mass of water vapor, R the universal gas constant with value 8.314 $JK^{-1}mol^{-1}$, M_{H_2O} the molar mass of water with value 18.01528 $g\,mol^{-1}$, T_{amb} is the ambient air temperature and T_d the dew point temperature measured by DPH. By transforming Equations 3.8 and 3.9 to mass per volume the two parameters in Equation 3.7 result in:

$$TWC(T_d) = \frac{m_{l,g}}{V_{l,g}} = \frac{E_{l,g} \cdot M_{H_2O}}{R \cdot T_d}$$

$$VWC(T_{amb}) = \frac{m_g}{V_g} = \frac{E_g \cdot M_{H_2O}}{R \cdot T_{amb}} \qquad \textbf{Equation 3.10}$$

and $CWC(T_d, T_{amb})$ can be calculated by subtracting these two equations above.

Furthermore, the ambient relative humidity (RH_{amb}) can be calculated with similar theory. For this case the saturation vapor pressure E_g of the corresponding dew point temperature T_d was used to calculate vapor pressure of ambient air (p_g). With the ideal gas law following relation is given:

$$p_g V_g = n_g R T_{amb} \qquad \textbf{Equation 3.11}$$

$$p_{l,g} V_{l,g} = n_{l,g} R T_d$$

Given that $n_{l,g}/V_{l,g}$ and n_g/V_g have the same values Equation 3.11 can be simplified and the partial vapor pressure from ambient air can be calculated:

$$p_g = \frac{T_{amb}}{T_d} p_{l,g} \qquad \textbf{Equation 3.12}$$

In Equation 3.12 $p_{l,g}$ is equal to the saturation vapor pressure of the liquid and gas mixture as T_d is used. By calculating saturation vapor pressure for ambient air (water in gas phase) E_g with using ambient temperature and the parameterization coefficients given in Table 2.1 one can calculate the ambient relative humidity RH_{amb} just as a function of T_{amb} and T_d:

$$RH_{amb}(T_d, T_{amb}) = \frac{p_g}{E_g} \qquad \textbf{Equation 3.13}$$

Summary of CWC formulas

This short section summarizes the two formulas mentiones above to calculate CWC and RH_{amb} from the T_d measured by a DPH connected behind total inlet, and ambient temperature T_{amb}.

The coefficients a_x of Equation 3.14 and 3.15 are listed in Table 2.1.

$$CWC(T_d,T_{amb}) = \frac{a_0 + a_1T_d + a_2T_d^{\,2} + a_3T_d^{\,3} + a_4T_d^{\,4} + a_5T_d^{\,5} + a_6T_d^{\,5}}{R \cdot T_d} - \frac{a_0 + a_1T_{amb} + a_2T_{amb}^{\,2} + a_3T_{amb}^{\,3} + a_4T_{amb}^{\,4} + a_5T_{amb}^{\,5} + a_6T_{amb}^{\,5}}{R \cdot T_{amb}} \qquad \textbf{Equation 3.14}$$

$$RH_{amb}(T_d,T_{amb}) = \frac{\frac{T_{amb}}{T_d}\left(a_0 + a_1T_d + a_2T_d^{\,2} + a_3T_d^{\,3} + a_4T_d^{\,4} + a_5T_d^{\,5} + a_6T_d^{\,5}\right)}{a_0 + a_1T_{amb} + a_2T_{amb}^{\,2} + a_3T_{amb}^{\,3} + a_4T_{amb}^{\,4} + a_5T_{amb}^{\,5} + a_6T_{amb}^{\,5}} \qquad \textbf{Equation 3.15}$$

3.2. Calculating the ambient peak supersaturation

Measuring the ambient peak supersaturation SS_p within a cloud is not possible and has to be retrieved from other measurement parameters. With the measurement setup during the CLACE2010 campaign there is a possible way to calculate the SS_p:

The ambient activation diameter $D_{50,amb}$ can be calculated with the number of hydrometeors (e.g. measured by a FM) and total aerosol size distribution (e.g. measured by an SMPS). To link the ambient activation diameter with SS_p one has to consider measurements of a cloud condensation nuclei counter (CCNC)[1]. For every preset SS in the CCNC one gets the number of CCN. The number of CCN is used to add up in the total aerosol size distribution by starting at largest size until $D_{50,SS}$ is found (see Fig. 3.6). This $D_{50,SS}$ value is only valid for a certain SS given by the CCNC. By calculating $D_{50,SS}$ values for every preset SS, an adequate fitting function $f(D_{50,SS}) = SS(D_{50,SS})$ can be retrieved. Inserting the calculated $D_{50,amb}$ retrieved by adding up the total aerosol size distribution starting at largest size with number of measured hydrometeors SS_p can be calculated.

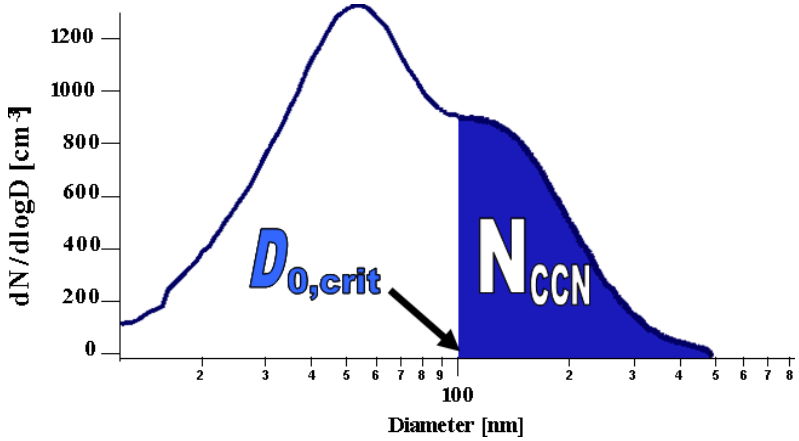

Fig. 3.6: Size distribution from the SMPS at the Jungfraujoch connected to the total inlet. In blue area the idea for adding up to number of cloud droplets is shown.

[1] Further explanations about the CCNC can be found in ROBERTS & NENES (2005) or JURÁNYI (2010).

The calculated supersaturations will be verified with statistical analyses. The actual cloud formation and type have to be considered by comparing the supersaturations due to the duration of a SMPS (6 minutes) and a CCNC (~60 minutes) scan. Thus, an adequate cloud period criterion has to be established.

3.3. Establishing a Cloud Period Criterion

Liquid water content (LWC) within a cloud is highly fluctuating due to spatial inhomogeneity in cloud, evaporation/condensation and the collision of interstitial aerosols with cloud droplets (SEINFELD & PANDIS, 2006). Wind fluctuations within clouds play also a major role in fluctuation of LWC. To define whether a cloud was present during one SMPS scan of 6 minutes or not, an adequate cloud period criterion has been retrieved for CLACE2010.

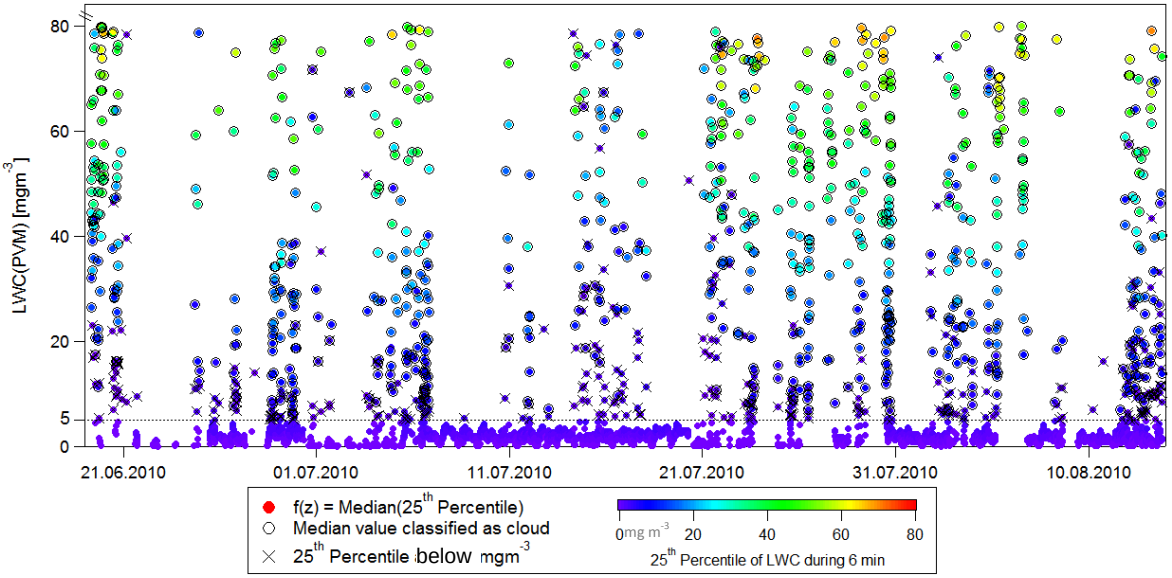

Fig. 3.7: To establish an adequate cloud period criterion, median LWC values were depicted as function of the corresponding 25th-percentile (different colors of points). If the median value *and* the 25th-percentile of LWC during 6 minutes (one SMPS scan) were above the threshold of 5 mg m^{-3} the dots are circled. If median value is above and the 25th-percentile is below 5 mg m^{-3} the dot is depicted with a cross. Thus, colored dots depicted with a circle or cross were correctly classified as a cloud period. If dots have a circle *and* a cross the period has been misclassified. Best results have been achieved with the criterion that 70% of the time LWC must be above 5 mg m^{-3} (30th percentile).

HENNING (2002) found a cloud period criterion that classifies the conditions as cloudy if LWC is higher than 20 mg m^{-3} for more than 85% of an hour. However, for this study only one SMPS system was operated and was connected behind a switching inlet (interstitial and total inlet). As mentioned above, during CLACE2010 two SMPS systems were used and connected to total and interstitial inlet, respectively. Thus, a better time resolution could be achieved than in the study of HENNING (2002) and a less strong cloud period criterion can be used.

The criterion for a stable cloud period is defined such that the 25th-percentile *and* the median of LWC over 6 minutes (one SMPS scan) must lie above the defined threshold. Fig. 3.7 shows the median values of LWC averaged over 6 minutes. Different colors indicate the corresponding 25th-percentiles. For better readability median values classified as a cloud period are depicted in circles and values where the corresponding 25th-percentile lies below the threshold are marked with a cross. Best results were achieved by setting the threshold such that during 70% of the time LWC must lie above 5 mg m^{-3}.

3.3.1. Convective cloud period criterion

To compare updraft velocities with SS_p a further criterion has to be established which distinguishes between convective clouds and other cloud types. For this issue the adiabatic lapse rate is a useful measure for classifying convective clouds. For a neutral, water-free atmosphere the temperature decreases by approximately -0.98 K per 100 m altitude (ANDREWS, 2010). This value is called the *dry adiabatic lapse rate*. If relative humidity exceeds 100% water will begin to condense on the available particles and latent heat of the water condensation process will be released. Latent heat released leads to a warming of the surrounding air and thus, the adiabatic lapse rate decreases and is now termed *moist adiabatic lapse rate*. Since the saturation vapor pressure of water is strongly dependent on temperature (see section 2.2), moist adiabatic lapse rate depends on temperature as well (SEINFELD & PANDIS, 2006). Thus, there is no general adiabatic lapse rate available to use for the conditions at the Jungfraujoch.

At Kleine Scheidegg (2061 m asl) temperature measurements (T_{KLS}) with a Hygroclip (Rotronic) device were conducted by the PSI. The temperature gradient dT/dz can be calculated with temperature measured at the Jungfraujoch (T_{JFJ}) by MeteoSwiss.

$$\text{lapse rate} = \frac{dT}{dz} = \frac{T_{JFJ} - T_{KLS}}{3580\,\text{m} - 2061\,\text{m}} \cdot 100 \left[\frac{\text{K}}{100\,\text{m}}\right] \qquad \textbf{Equation 3.16}$$

A criterion for a convective cloud period was found for values of $dT/dz < -0.7\,\text{K}/100\,\text{m}$ applying the assumption that during convective cloud periods a relative humidity of 100% is exceeded over the whole distance from Kleine Scheidegg to Jungfraujoch.

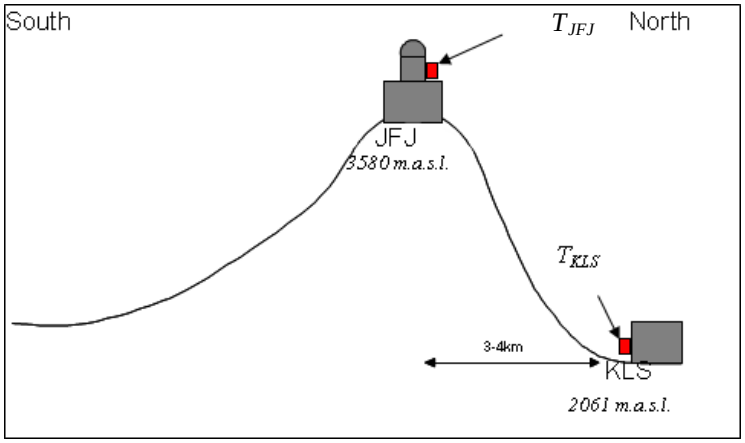

Fig. 3.8: Sketch of temperature measurements at the Jungfraujoch (JFJ) and Kleine Scheidegg (KLS). Temperatures measured at JFJ and at KLS are indicated with T_{JFJ} and T_{KLS} respectively.

4. Results and Discussion

4.1. Meteorological Conditions

The weather conditions during the CLACE2010 campaign at the Jungfraujoch can be divided into three different phases: the beginning of the campaign, the month of July and the end of the campaign. At the beginning of the campaign, during June, the phenomenon *Schafskälte* was dominant. This corresponds to very cold days in June accompanied by snowfall in mountain regions. This time period is associated with low air pressure and low temperatures, which can be seen in Fig. 4.1, during the second half of June. By the beginning of July a strong Azores high was dominating the weather in Switzerland for almost the whole month of July. Every few days high-pressure systems separated from the Azores high and kept the air temperature at a high level. Thus, only few convective clouds were present during this period and solar radiation was, relative to previous years, very high. After the passage of a high-pressure area, thunderstorms occurred due to the arrival of humid and unstably layered air (see Fig. 4.1).

By the end of July, the Azores high gradually dissolved and several fronts arrived at the Jungfraujoch until the end of the campaign. These fronts caused high levels of precipitation and with decreasing temperature increasingly more snowfall occurred. Solar radiation decreased to normal conditions for Jungfraujoch.

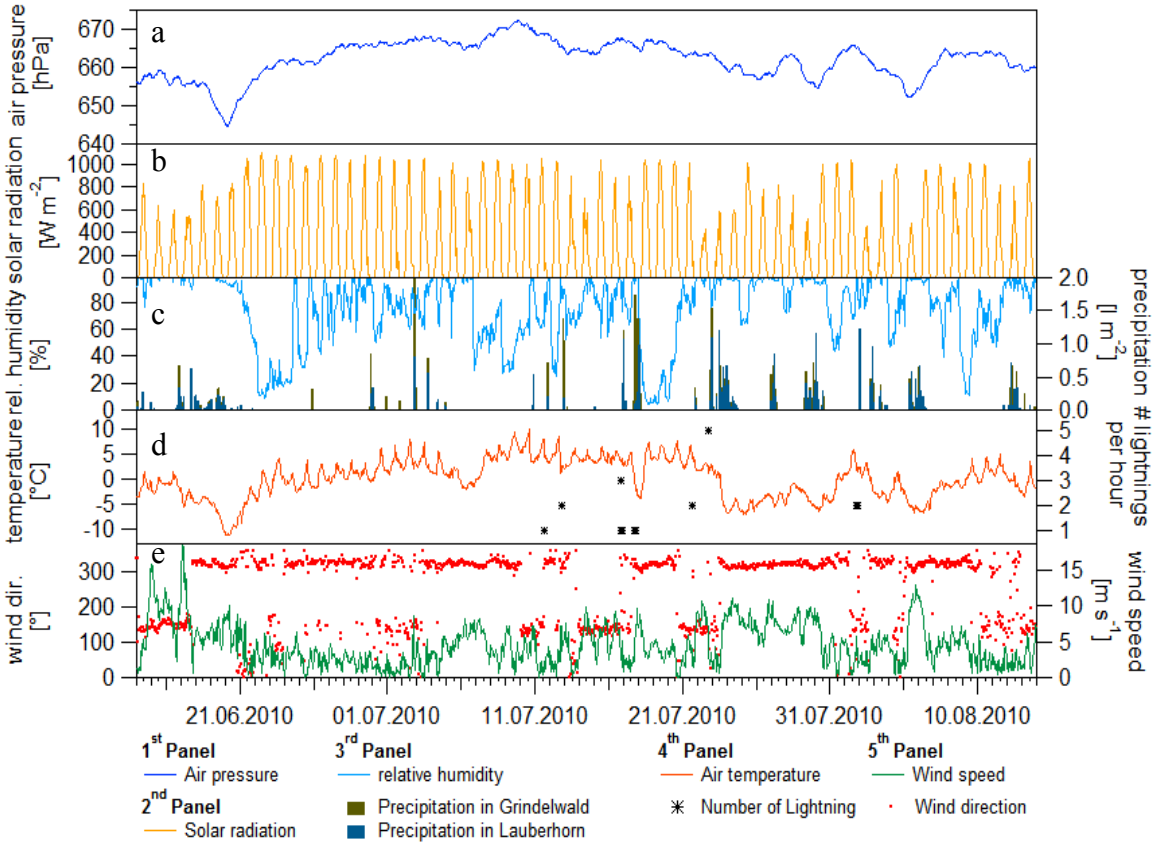

Fig. 4.1: A collection of several meteorological data during whole CLACE2010 campaign in hourly averages measured by MeteoSwiss: a) Air pressure. b) Global radiation. c) Relative humidity in light blue and precipitation of two different stations nearby Jungfraujoch: Grindelwald (green) and Lauberhorn (blue). (data source: *MeteoMedia*) d) Ambient air temperature (orange) and number of lightnings per hour detected within a radius of 3km around Jungfraujoch. e) Wind direction (red) and wind speed (green) around Jungfraujoch.

During the whole campaign the dominating wind direction was around 340° and wind speed was mostly in the range of 0 to 10 ms^{-1}.

4.2. Data Validation

As shown in Fig. 4.1, temperature was quite low at the beginning and the end of CLACE2010. This led to problems due to freezing of some devices especially the FM and the sonic anemometer. In Fig. 4.2 the data coverage of used instruments during the whole measurement campaign is shown for every day. The sonic anemometer delivered 75% and the FM 87% data during the whole campaign. The interstitial SMPS delivered 100% valid data (not shown), whereas the total SMPS recorded 96% and the PVM 98% valid data during CLACE2010.

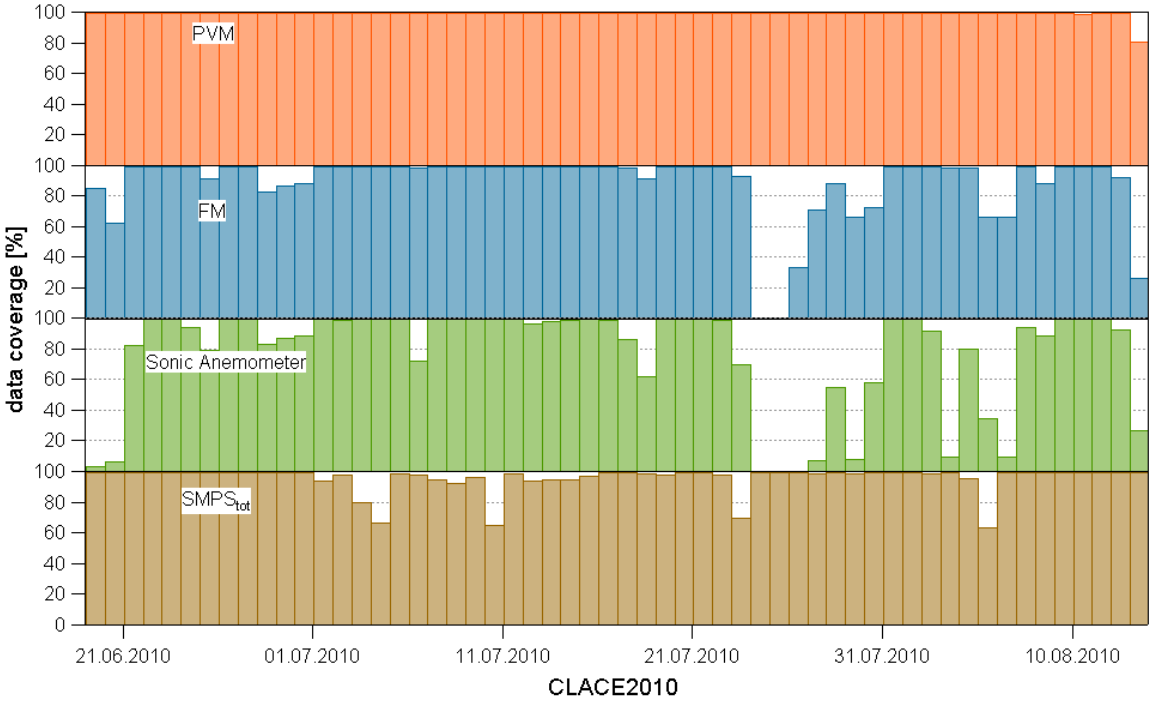

Fig. 4.2: Valid data availability is shown for following devices: particle volume monitor (PVM), fog monitor (FM), sonic anemometer and Scanning Mobility Particle Sizer (SMPS).

4.2.1. Number concentration of activated aerosols

During the intensive measurement campaign CLACE2010, additionally to the total inlet an interstitial inlet was installed. The difference between the total number concentrations from the two SMPS ($N_{tot\text{-}int}$) gives the number of CCN that were activated before the drying process of the total inlet occurred. Thus, $N_{tot\text{-}int}$ can be compared to the number concentration of cloud droplets measured by the FM. Fig. 4.3 shows the relationship between the number of activated cloud condensation nuclei (CCN), calculated by the difference of the number concentration measured by the total and the interstitial SMPS ($N_{tot\text{-}int}$), and the number of cloud droplets measured by the FM. Periods where horizontal and vertical wind direction relative to FM were not within the range of ±45° have been neglected. Only data during cloud periods (see section 3.3) have been taken into account.

A few data points agree quite well with each other. Nevertheless, a quite large data cloud can be seen below and above the logarithmic 1:1-line. The large difference between the two measuring methods are most likely the result of low ambient temperatures (below 0°C). As already mentioned in section 4.1 quite cold temperatures were measured at the beginning and

the end of CLACE2010. A heavy freezing of the FM inlet during these periods was regularly observed by eye. It may well be that supercooled cloud droplets froze onto the inlet of the FM and therefore inhibited the flow of cloud droplets into the device. A good argument for this issue is the good agreement of data during warm cloud periods. However, a non-negligible amount of values measured by the FM is higher compared to SMPS measurements. This feature is especially present in lower total number concentrations. A possible explanation for this feature could be that optical windows (part of the FM where the size of the cloud droplets is measured) were covered with ice. These periods have ambient temperatures quite strongly below 0°C. Periods where no hydrometeors could pass the inlet due to heavy freezing was also present but not shown in Fig. 4.3. Another reason could be the occurrence of less dense clouds since these periods correspond to an *LWC* below 200 mg m^{-3} and have therefore, a low counting statistics. At low concentrations ($N_{tot\text{-}int}$ < 10-20 cm^{-3}) also the SMPS measurements showed an increased uncertainty, originating from the cross-comparison of the instruments and poorer counting statistics.

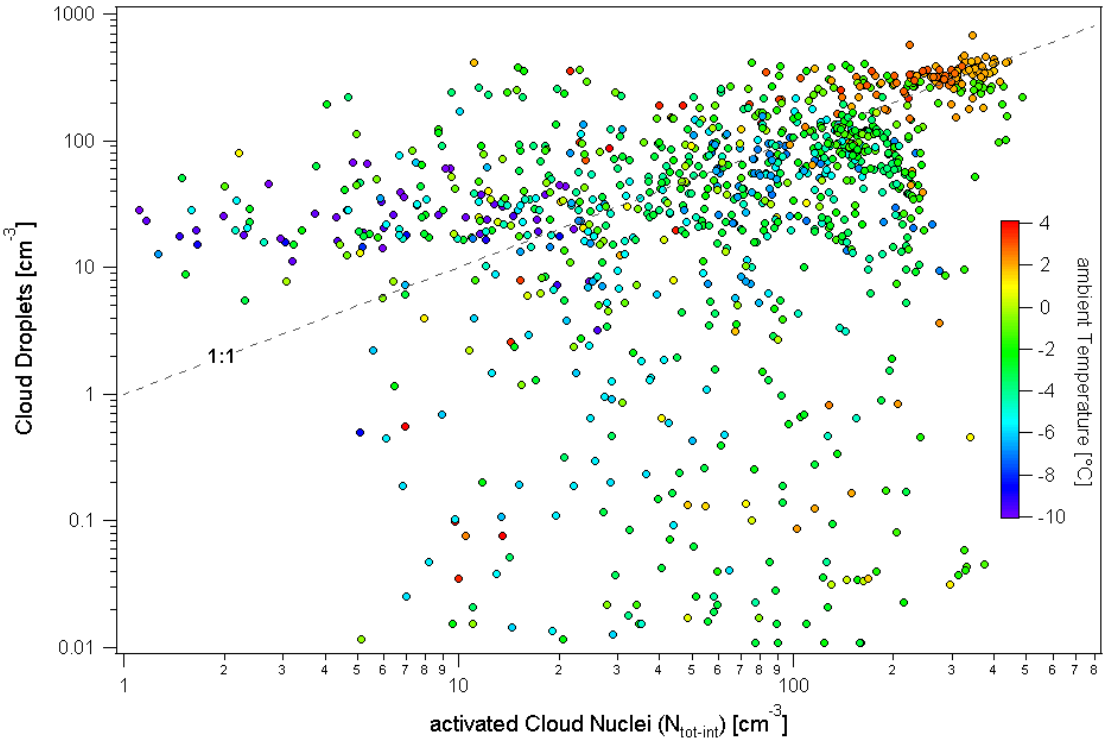

Fig. 4.3: Correlation between the number of activated cloud condensation nuclei calculated by the difference of total minus interstitial SMPS ($N_{tot\text{-}int}$) and the number of cloud droplets measured by FM. Different colors indicate prevailing ambient temperature.

4.2.2. Liquid water content

LWC measured by the FM and the particle volume monitor (PVM) are shown in the 4th panel of Fig. 4.4. It shows a randomly chosen cloud period during CLACE2010. A large difference between the LWC measured by FM and PVM can be seen. The difference was first expected to result from a non-convenient wind field, despite of the reinstallation of the FM with a steeper inclination. By considering the 1st and 2nd panel in Fig. 4.4 one can see that the horizontal wind directions as well as the vertical wind directions are quite often in the validity range of ± 45°. The absolute wind speed (depicted in 3rd panel of Fig. 4.4) shows a better explanation for the difference of both measured LWC values. Nevertheless, it has to be validated whether PVM or FM measured correctly. For that purpose, the condensed water content (CWC) has been calculated from the dew point hygrometer (Dewmaster Chilled

Mirror Hygrometer; Edgetech) by considering the theory of Clausius-Clapeyron (see section 2.2).

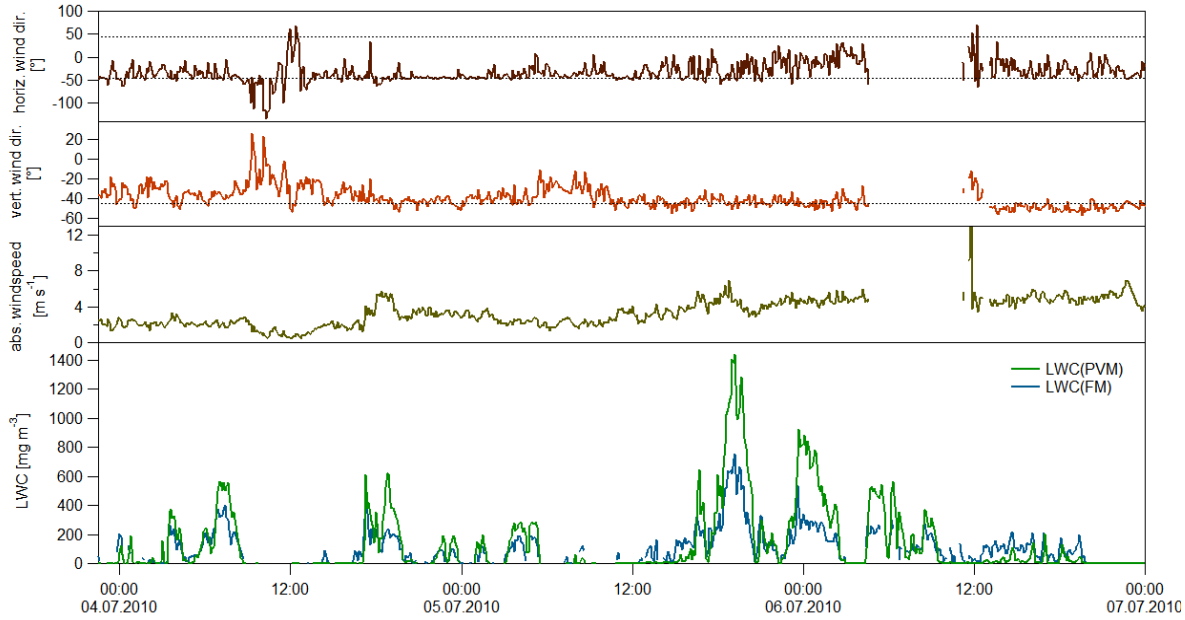

Fig. 4.4: In the 1st and 2nd panel horizontal and vertical wind direction are shown relatively to the inlet of the fog monitor. The absolute wind speed in the 3rd panel has been calculated as the root mean square of all three components given by the sonic anemometer. In the 4th panel the liquid water content from the particle volume monitor (PVM) and the fog monitor (FM) is depicted.

4.2.3. Calculating the Condensed Water Content

Behind the total inlet a dew point hygrometer (DPH) (Dewmaster, Edgetech) was installed in the laboratory, which measured the dew (or frost) point temperature of the total aerosol. Another DPM is operated by MeteoSwiss and is installed outside. The comparison between the dew point temperature measured by the two DPH instrument from MeteoSwiss (x-axis) and PSI (y-axis), respectively, showed a quite good agreement during cloudfree periods with a linear slope of 0.82 and a R^2 of 0.92. Only cloud free periods were considered due to the difference in measuring methods. The DPH from PSI measured behind the heated inlet so that during cloud periods it should have measured a higher T_d due to measuring the evaporated cloud droplets as well.

During CLACE2010 the condensed water content (CWC) can be assumed as the same value as the total water content or LWC due to the fact that during summer almost only warm clouds appeared and a negligible amount of mixed or iced clouds were present at the Jungfraujoch. Thus, either LWC measured by the PVM or measured by the FM should have the same value as the calculated CWC.

In Fig. 4.5 the CWC has been calculated by considering Table 2.1 to calculate the saturation vapor pressure over water and ice respectively. Negative values of CWC result from periods where clouds were not present. During such periods higher vapor pressures than liquid water were found in ambient air.

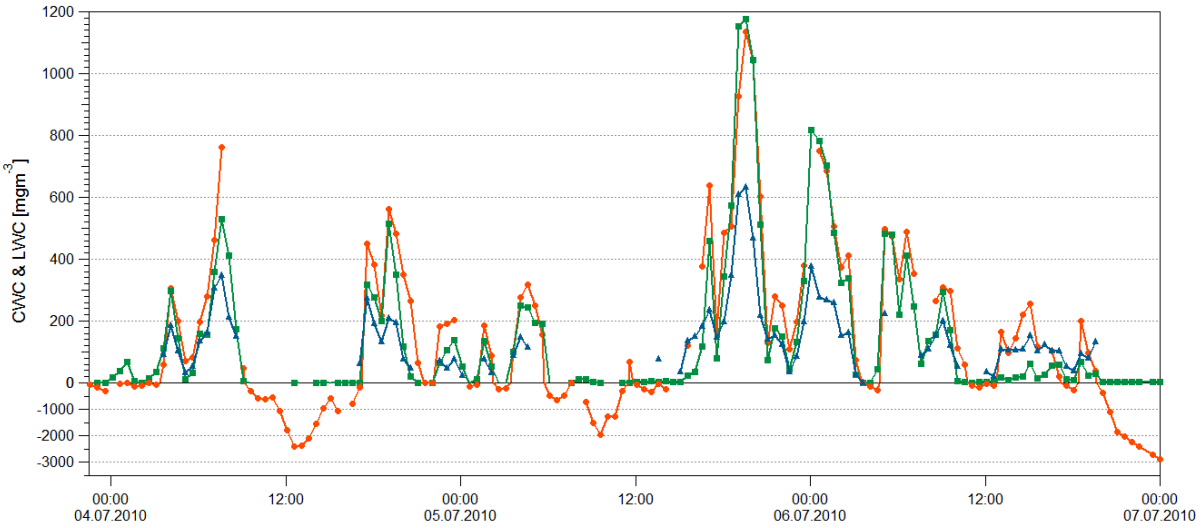

Fig. 4.5: Liquid water content measured by PVM (green) and FM (blue) are depicted together with the calculated CWC from DPH (orange). Data is averaged over 30 minutes.

The linear correlation coefficient between the LWC measured by the PVM and the calculated CWC has a value of 0.93 and a logarithmic R^2 of 0.54.

For further validation RH_{amb} was calculated (for explanations see section 3.1.6) to compare these values with RH measured by MeteoSwiss. Fig. 4.6 shows the calculated relative humidity RH_{amb} and the relative humidity measured by MeteoSwiss. A quite good agreement between these two parameters is found. Values above 100% of relative humidity are a result of the calculation which includes cloud water as well. Those values show the fraction of cloud water within the air parcel. For example a value of 120% means that the cloud consists of 20% of water (in terms of vapor pressure).

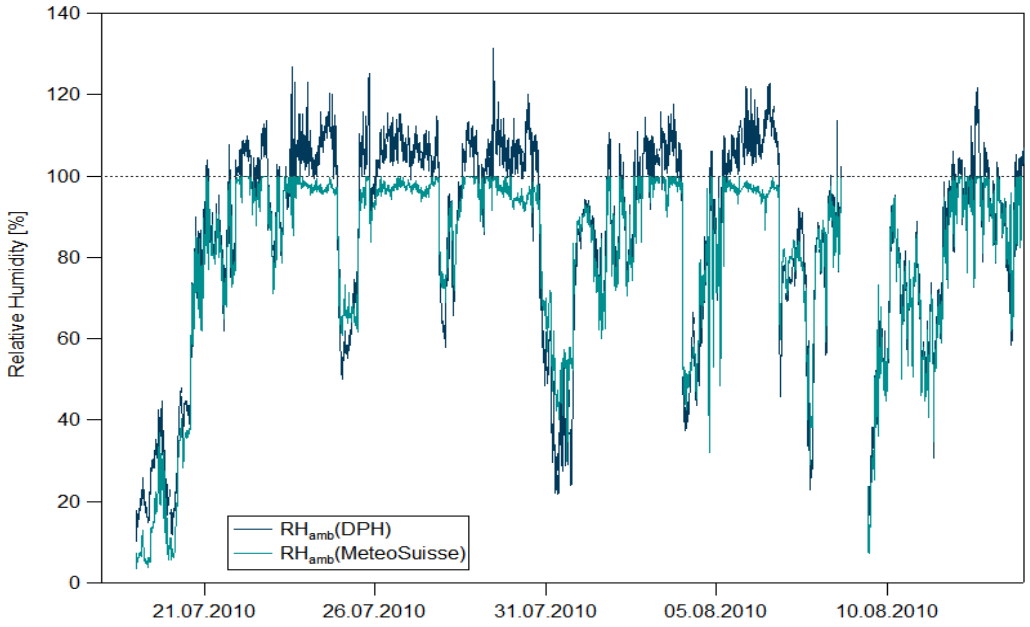

Fig. 4.6: Relative humidity RH from ambient air measured by the dew point hygrometer from MeteoSwiss and calculated by chilled dew point hygrometer from PSI.

4.2.4. Cloud periods

Applying the established cloud period criterion it has been found that 27% of time during the CLACE2010 campaign clouds were present. Compared to another method of classifying cloud periods (looking directly at different activation curves) the criterion used in this study showed an agreement with 3% difference. Thus, the established cloud period criterion mentioned in section 3.3 seems to be a good choice. For the second method of classifying stable cloud periods, an analysis was performed for the activated fraction of particles. The activated fraction of particles is a size-dependent process and is defined as (VERHEGGEN ET AL., 2007):

$$F_N(D_p) = \frac{(N_{tot}(D_p) - N_{\text{int}}(D_p))}{N_{tot}(D_p)} \qquad \textbf{Equation 4.1}$$

Since the size-dependent fraction is a normalized difference noisy data will dominate activated fraction at small numbers (often dominant at small particles as can be seen in Fig. 4.7).

Despite of the good agreement of the two methods classifying stable cloud periods, errors may occur due to low activated fractions of aerosols together with high LWC, as can be seen in Fig. 4.7. Hence, high LWC values must not always coexist with highly activated fractions of aerosols. In Fig. 4.7b it can be seen that despite of high LWC values the activated fraction remains quite low. Although LWC values are quite equal in Fig. 4.7a and b the CCN number concentration for the example on 17 July is less than half as the example of 24 July shows.

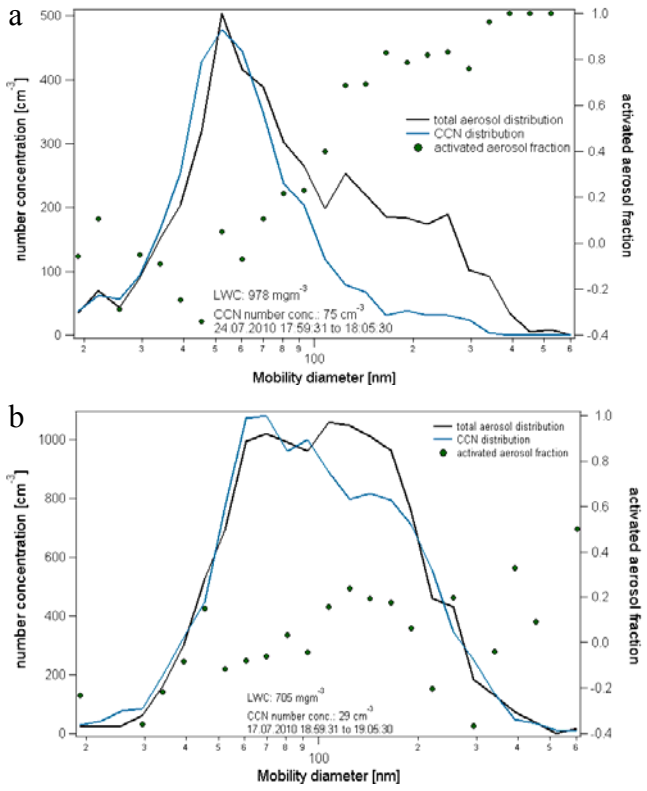

Fig. 4.7: Total aerosol size distributions and interstitial (CCN) size distributions. a) shows an example where a high activated fraction together with high LWC values occurred. b) shows a low activated fraction despite of high LWC values.

4.3. D_{50} dependence on LWC and air temperature

From Fig. 4.8 it can be concluded that there is a correlation between LWC and calculated activation diameter D_{50} as found in earlier studies (HENNING, 2002). Due to the high variability of clouds, only values for stable conditions have been used (see section 3.3). During less dense cloud periods (low LWC values) D_{50} decreases with increasing LWC up to 150 mg m^{-3}. Compared to HENNING (2002) during CLACE2010 the D_{50} stabilized at lower LWC values and was never as high. It has already been found that in the accumulation mode, the particle number concentration influences D_{50} as well. At low number concentrations, particles with diameters smaller than 100 nm were also activated.

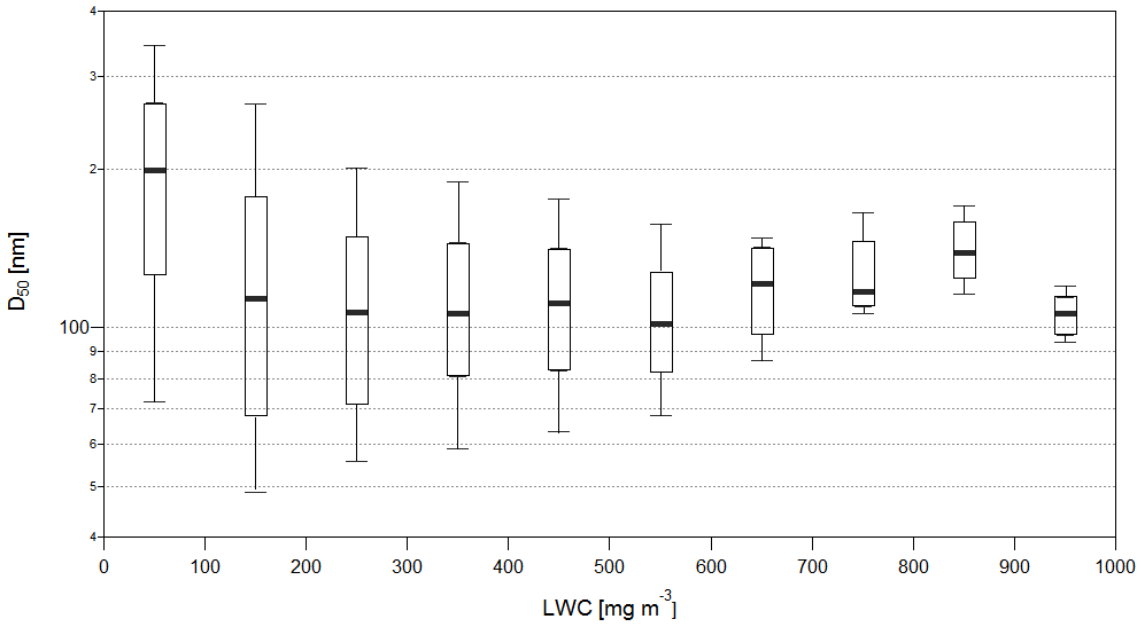

Fig. 4.8: Activation diameter *D50*, with 10th, 25th, median, 75th and 90th percentile, versus LWC classes during CLACE2010 for cloud periods only (LWC 70th percentile > 5 mg m-3).

Considering the meteorological conditions during the campaign, measured air temperature showed a wider range than in HENNING (2002). Thus, it can be expected that the much lower values of D_{50} during CLACE2010 compared to the earlier campaign resulted from a dependence of D_{50} on air temperature T_{air}. In Fig. 4.9 this issue is shown as a function of T_{air} and LWC. It can be concluded that D_{50} values with LWC > 150 mg m^{-3} (not shown) are less dependent on air temperature. When T_{air} is larger than 0°C D_{50} slightly increases with increasing temperature. At T_{air} < 0°C D_{50} seems to remain constant independent of the LWC. For LWC < 150 mg m^{-3} the data is noisy and has larger D_{50} values than shown before in Fig. 4.8. A possibility for the dependence of D_{50} on T_{air} could be that during periods while T_{air} > ~0°C injections of planetary boundary layer (PBL) was more dominating so that less hygroscopic particles (due to freshly emitted aerosols) could reach the Jungfrujoch (JURÁNYI ET AL., 2011 in press). This would result in lower SS_p and thus higher D_{50}. Another possibility for the increase in T_{air} with increasing D_{50} could be that saturation vapor pressure within an air mass increases with increasing T_{air} (due to Clausius-Clapeyron theory) and thus SS_p would decrease.

At T_{air} < 2.5°C D_{50} seems to slightly increase again. The Kelvin effect together with the two possiblities described before may explain this issue. While T_{air} decreases the Kelvin effect becomes more important and the critical supersaturation within droplets will increase and D_{50} will decrease. Since the saturation vapor pressure within an air mass decreases with

decreasing temperature SS_p is expected to increase if vapor pressure remains constant and the ambient critical diameter should decrease. Thus, D_{50} may be inhibited to increase by the Kelvin effect although more hygroscopic particles were present since no injections of the PBL are expected at $T_{air} < 0$°C.

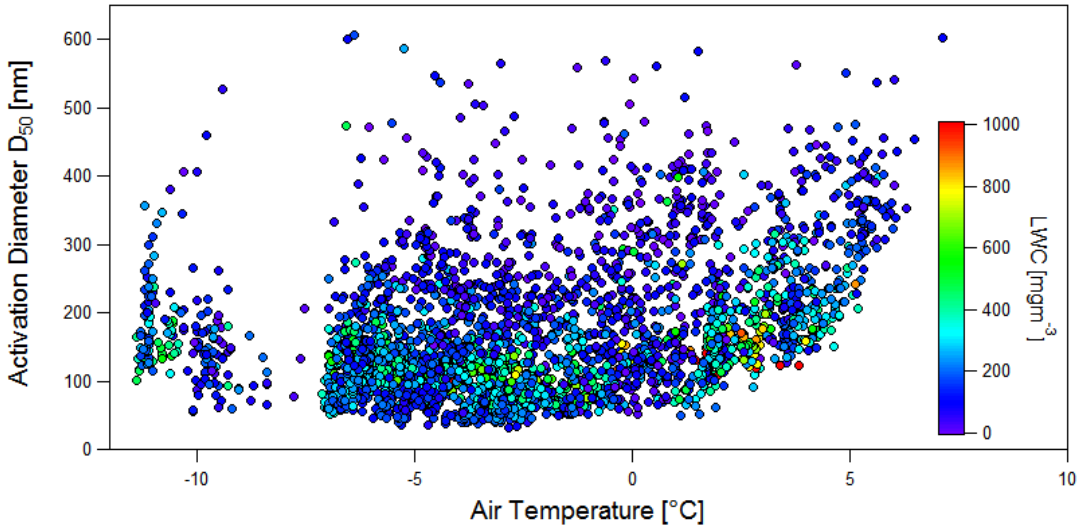

Fig. 4.9: Scatter plot of activation diameter D_{50} versus air temperature as function of LWC (different colors). Only values for 30th percentile of LWC higher than 5 mg m^{-3} were used.

4.4. Ambient peak supersaturation

Due to an unknown reason the CCNC instrument delivered slightly too high number concentrations during the CLACE2010 campaign so that data could not be used (see Appendix B.). To calculate SS_p as described in section 3.2, a CCN climatology of the Jungfraujoch was used to calculate D_{50} (JURÁNYI ET AL., 2011 in press). Since the chemical composition of particles at the Jungfraujoch is quite constant (KAMMERMANN ET AL., 2010) the use of a CCN climatology seems to be valid for further analysis. Fig. 4.10 shows calculated D_{50} over 17 months for four different supersaturations (SS) measured by a CCNC at the Jungfraujoch. It can be seen that D_{50} for a given SS remains nearly constant over the whole 17 months. Thus, the climatology of CCN number concentration at the Jungfraujoch seems rather a good possibility to calculate SS_p.

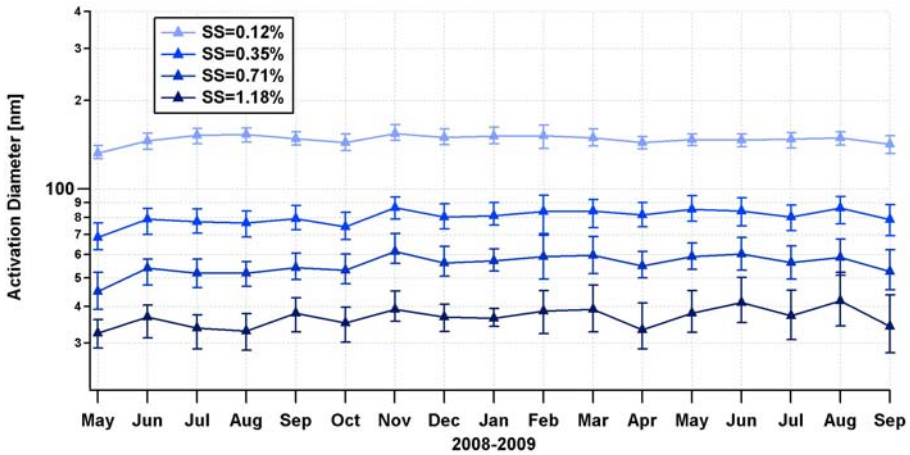

Fig. 4.10: Calculated median values of activation diameter (D_{50}) with 25th and 75th percentile over 17 months for four different supersaturations measured by CCNC (JURÁNYI et al., 2011 in press).

The 25th, median and 75th percentiles were calculated over all 17 months and were plotted against the corresponding *SS*. The most adequate fitting function for this issue was a power fit (see Fig. 4.11):

$$D_{50} = f(SS_p) = y + A \cdot SS_p^{\,p} \qquad \textbf{Equation 4.2}$$

where *y*, *A* and *p* are fitting coefficients. In Fig. 4.11 it can be seen that the power fit function represents all measured *SS* well. Only the largest value of *SS* = 1.18% seems to slightly deviate from the fitting function. This deviation could result in somewhat smaller *SS* values for lower D_{50} values. High D_{50} values show a quite small inner-range of the three power fit functions. With *SS* values smaller than 0.07% one could see that the three power fit functions crossed each other so that resulting *SS* values values would be physically not reasonable. Thus, *SS* values smaller than 0.07% have been neglected for further analysis.

Due to the freezing of the FM, number concentration of ambient CCN calculated from the difference of total and interstitial SMPS were used. Transforming Equation 4.2 to *SS* and applying the calculated D_{50} leads to calculated SS_p. In Fig. 4.12 mean and median value, 10th, 25th, 75th and 90th percentile of calculated SS_p are shown for the three different D_{50} scenarios retrieved from climatology (JURÁNYI ET AL., 2011 in press). The 25th (high hygroscopicity) and 75th (low hygroscopicity) percentiles of climatology of D_{50} have been used to gain more knowledge about the influence of D_{50} on SS_p values.

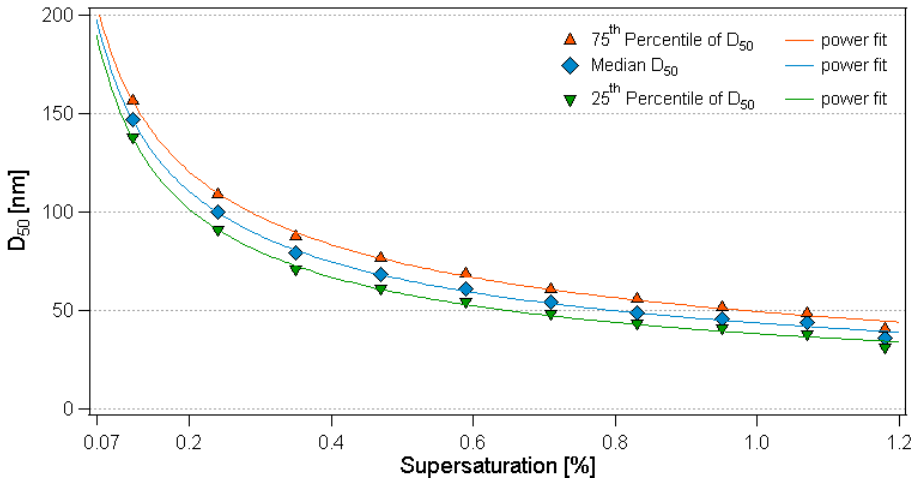

Fig. 4.11: Power fit functions (see Equation 4.2) of 25th, median and 75th percentiles of D_{50} and corresponding *SS*.

It was observed that SS_p values show a quite wide range. Thus, there is no certain SS_p value which characterizes the formation of clouds at the Jungfraujoch. During the CLACE2010 campaign an SS_p mean value of 0.26% and a median value of 0.17% have been found for intermediate hygroscopicity.

However, the slight decrease in the 10th percentile values of SS_p from high to low hygroscopicity show that this method still show some problems. Since this issue cannot be explained with errors in power fit functions, the temperature dependence of the calculated D_{50} could play the major role. D_{50} values calculated from both SMPS during the CLACE2010 campaign are strongly dependent on ambient air temperature. In contrast D_{50} values retrieved from climatology of CCNC were obtained on the quite constant laboratory temperature (~300 K). Kelvin's law (see Equation 2.7) says that particle activation is strongly dependent on the surrounding temperature as well. Thus, SS_p values at low ambient temperature could result in wrong calculated D_{50} due to a larger difference between ambient and laboratory

temperature. To consider this issue κ-values should be calculated for each cloud event. This problem or question will be tackled in a further study. Nevertheless, data is assumed as valid enough to do further analyse since already low SS_p values have been neglected.

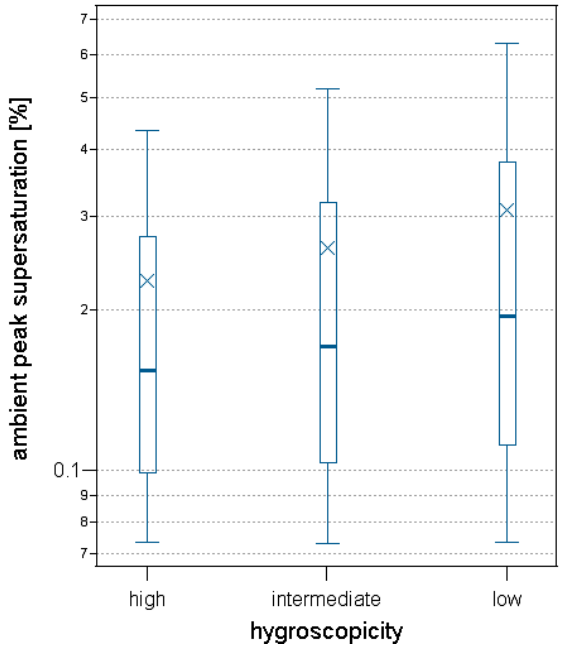

Fig. 4.12: Calculated peak supersaturations for stable cloud events (only values for the 30th percentile of LWC higher than 5 mg m^{-3} were used). SS_p values were calculated with climatology of D_{50} for the 25th (high hygroscopicity), median (intermediate hygroscopicity) and 75th (low hygroscopicity) percentile. The cross of ech boxplot depicts the mean value, the bold lines depicts the median and the other line show the 10th, 25th, 75th and 90th percentile.

It can be concluded that the correctness of measured D_{50} does not play a major role for calculating SS_p values due to the small deviations found for SS_p values with 25th (high hygroscopicity) and 75th (low hygroscopicity) percentile of D_{50} (relative error of D_{50} = ±13% and of SS_p = ±10%). Looking at the standard deviation band during stable cloud periods, strongly oscillating SS_p values (not shown) show larger standard deviations. However, these larger deviations still are in a quite small range compared to less oscillating SS_p. Thus, other parameters seem to have a much greater influence on SS_p values.

4.5. Dependence of SS_p on other parameters

From Fig. 4.8 it was concluded that there is a correlation between the LWC of stable cloud periods and calculated D_{50}. Hence, a correlation between LWC and calculated SS_p is also expected. Fig. 4.13 indicates a coexistence of decreasing air temperature with clouds. This confirms that when clouds arrive at the Jungfraujoch this corresponds with the arrival of cold air masses from the south or the north. Since cooling occurs at the arrival of almost every cloud type, a distinction between advection and convection cloud cannot be made. In section 4.5.1 the issue of differentiating between the two cloud types is treated.

No direct correlation between updraft velocities (w) and SS_p could be seen. With a logarithmized SS_p values (y-axis) and w (x-axis) the linear regression led to a slope of 0.02 and a R^2 of 0.03. One possibility for this issue again is that two cloud types were present at the Jungfraujoch: advection and convection clouds. The former type should lead to better correlations than the latter one. A second possibility for the weak correlation between w and SS_p could be that the location of activation of aerosols was not directly at Jungfraujoch where

the parameters for calculation of SS_p were measured. Nevertheless, other parameters seem to influence all cloud types at the Jungfraujoch.

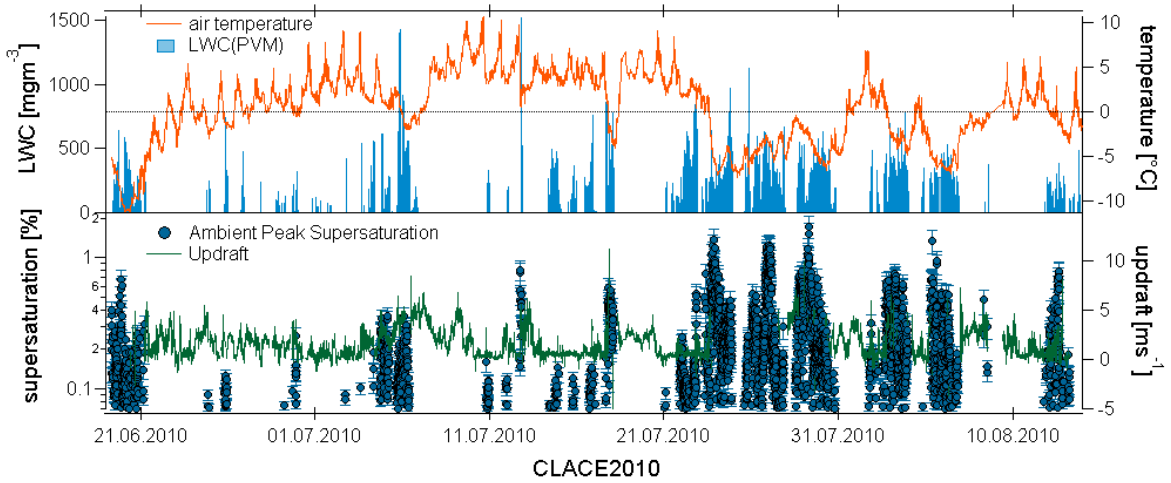

Fig. 4.13: Liquid water content (LWC) of clouds is shown with air temperature (upper panel). Calculated peak supersaturations (SS_p) are shown with updraft velocities (lower panel). Only values for 30th percentile of LWC higher than 5 mg m^{-3} were used over whole CLACE2010.

A decrease in air temperature has been found for almost every cloud period measured during CLACE2010. Referred to the quite strong correlation between D_{50} and air temperature for LWC > 150 mg m^{-3} shown in Fig. 4.9 a dependence of SS_p on air temperature can be shown from Fig. 4.14. An increase in air temperature corresponds to increasing values of SS_p up to ~-2°C. For temperatures larger than -2°C SS_p seems to decrease. A possible reason for the decrease in supersaturation with decreasing temperature could be the Clausius-Clapeyron relation. At low air temperature a given SS_p corresponds to a lower absolute water vapor concentration. Thus, activation at a certain number of particles causes a larger decrease in SS_p values at colder air temperatures. This issue is in quite good agreement with Verheggen et al. (2007). However, in the winter camapaign mentioned in this paper the decrease in activated fraction with decrease in air temperature has been explained more accurately with the Werner-Bergeron-Findeisen (WBF) process, while it is assumed that during CLACE2010 campaign only a small amount of ice is expected to be present (due to the summer campaign). Hence, the WBF process has only a small contribution to the explanation for the decrease in SS_p with decrease in air temperature. However, in a mixed-phase cloud there is a flux of water vapor from the liquid phase to the ice phase due to the lower saturation vapor pressure over ice than over liquid. This will lead to evaporation of recently formed cloud droplets and CCN will be released back into interstitial phase. Thus, the quite fast growth of ice particles leads to a decrease in SS_p. Either way, it is not yet quite clear if WBF or Clausius-Clapeyron explain this increase in SS_p values with increasing air temperature. Further research with a cloud box model my show reasons for this pattern.

The reverse trend observed at air temperatures above -2°C can be explained like Verheggen et al. (2007) did: The lower supersaturations with increasing temperatures above -2°C coincide with high total particle number concentration. The higher particle number concentration at higher air temperatures results in injections of more polluted air due to rising of PBL to the Jungfraujoch.

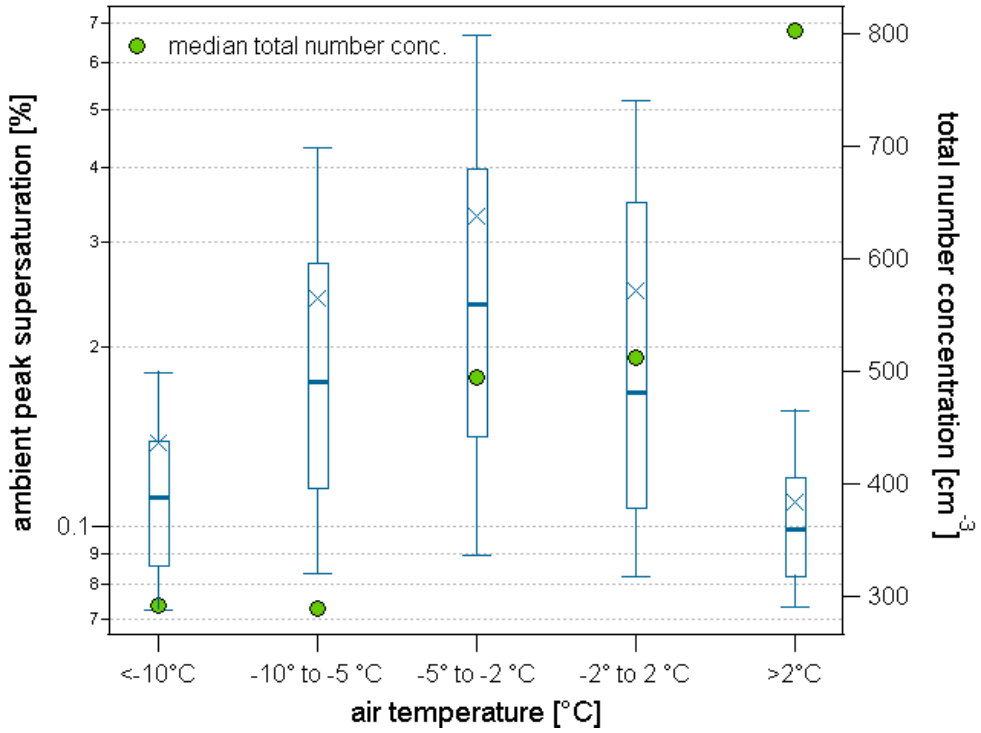

Fig. 4.14: Ambient peak supersaturation SS_p (mean and median value, and 10th, 25th, 75th, 90th percentile) versus air temperature classes for stable cloud periods (30th percentile of *LWC* higher than 5 mg m^{-3}). Green dots represent median values of particle total number concentration.

Median, 10th, 25th, 75th and 90th percentiles, and mean values of SS_p have been calculated for different PSA classes and have been related to each other (see Fig. 4.15).

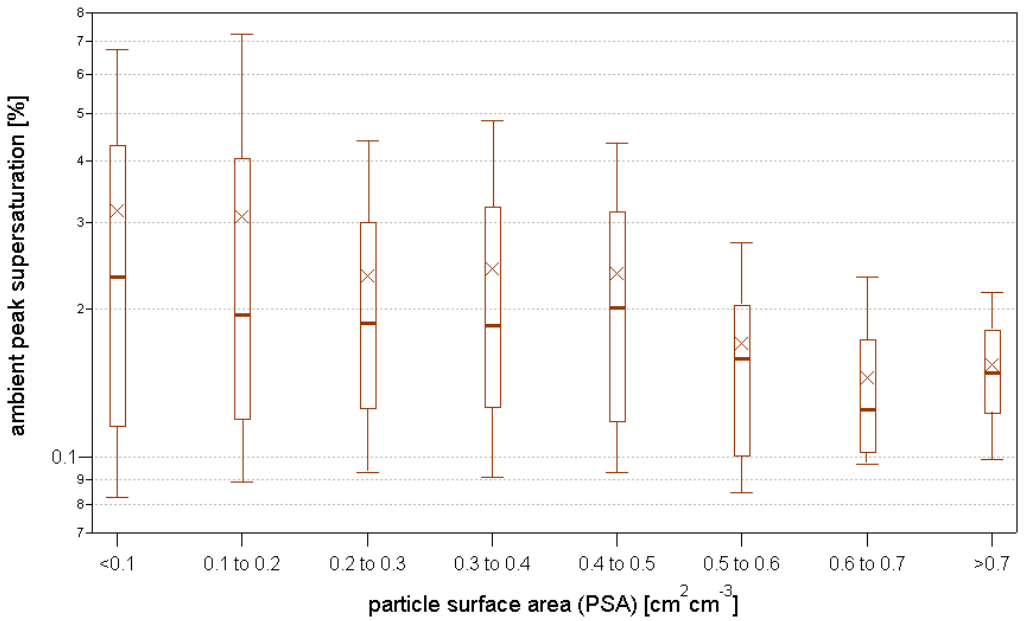

Fig. 4.15: Calculated ambient peak supersaturation (median and mean value, and10th, 25th, 75th, 90th percentile) versus particle surface area classes.

While median values SS_p for every PSA class seems to remain approximately constant, the mean values of SS_p decrease to PSA ~ 0.7 cm^2cm^{-3}. A decrease in SS_p with increasing PSA can be explained with a larger amount of activated aerosols pointing to less vapor pressure available. Thus, a slight decrease in SS_p values can be seen with increasing PSA values. This issue can be explained since more available surface for vapor to condense onto it leads to

faster vapor flux to the hydrometeors. Thus, SS_p cannot increase since a large amount of vapor immediately condenses onto the available surface.

SS_p dependence on regional wind direction

To get regional wind directions around the Jungfraujoch, data from MeteoSwiss has been used. Their device was installed at the tourist platform at a height of 10 m over ground so that regional wind field is representative for whole Jungfraujoch.

Considering SS_p values separated to air coming from north (270° < horizontal wind direction <90°) and south (130° < horizontal wind direction < 230°) a clear distinction can be made: while air coming from the north results in SS_p values of a quite wide range, SS_p values with air coming from the south are most often constant around 0.1% (see Fig. 4.16). The lower and constant SS_p values could be a result of air masses coming up over the Great Aletsch glacier and thus cooling down (dependent on temperature differences rather than on specific temperature). As mentioned before lower air temperatures lead to lower available vapor concentration. This result is in quite good agreement with Verheggen et al. (2007). This study showed that a lower number concentration is a result of less injections of PBL air. Since air masses coming from the south are more polluted, the available water vapor can be distributed faster to the particles and thus SS_p remains on a low level. The median values of the total particle concentration for south and north during CLACE2010 are $N_{tot,south}$=771 cm^{-3} and $N_{tot,north}$=279 cm^{-3}. The larger variability in SS_p with air coming from the north is most likely due to more turbulence caused by topography. While the south of the Jungfraujoch has a nearly smooth topography, the north shows much more influences on wind stream due to several valleys and mountains. Another possibility could be that from south only advection clouds are possible and thus SS_p is low due to expected small w.

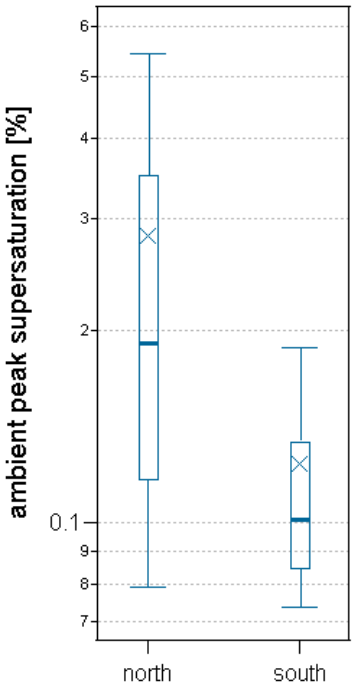

Fig. 4.16: Ambient peak supersaturations have been separated to the horizontal wind direction measured at the Jungfraujoch. North conditions are classified while measured horizontal wind direction *ss* was in a range of 270° < *ss* < 90°. South conditions are classified with 130° < *ss* < 230°. Cases from the south: 235 and from the north: 2002

4.5.1. Distinction between advective and convective cloud types

So far all stable cloud periods with the 30th percentile of *LWC* larger than 5 mg m^{-3} have been considered. From Fig. 4.13 it could be shown that stable cloud periods can be distinguished into two major cloud types: advection and convection clouds. Convection clouds coexist with an increase in *w* and SS_p values, while advection clouds have small *w*. This means that aerosols in convection clouds should have been activated during the ascent of the air masses from the Kleine Scheidegg to the Jungfraujoch. Aerosols within advection clouds could have activated either in air masses above the Kleine Scheidegg or much further away.

In Fig. 4.17 prime examples for advection and convection clouds, respectively, are shown. For advection clouds a slight decrease of SS_p at arrival of the cloud is visible and a fast increase in SS_p followed by quite constant values was observed. Thereby, *w* remained at an approximately constant low level. On 12 July, 2010, advection clouds were observed at the Jungfraujoch. While temperature decreased quite fast, an increase in *w* and in SS_p was measured. At the same time as *w* decreased, SS_p values decreased together with LWC values as well.

Additional to stable cloud periods, the criterion described in section 3.3.1 was applied to the data. Fig. 4.18 shows the calculated SS_p versus *w* (it is important to note that *w* has been measured locally at the Jungfraujoch and is not directly located where cloud formation actually occurred). A difference has been made with air parcels coming from the north (green diamonds) and the south (blue dots). Since the location of the sonic anemometer gives just representative data for wind coming from the north (R^2=0.31, *w*: x-axis and SS_p: y-axis), SS_p during south-wind conditions do not correlate (R^2=0.06, *w*: x-axis and SS_p: y-axis) with *w* measured from the sonic anemometer.

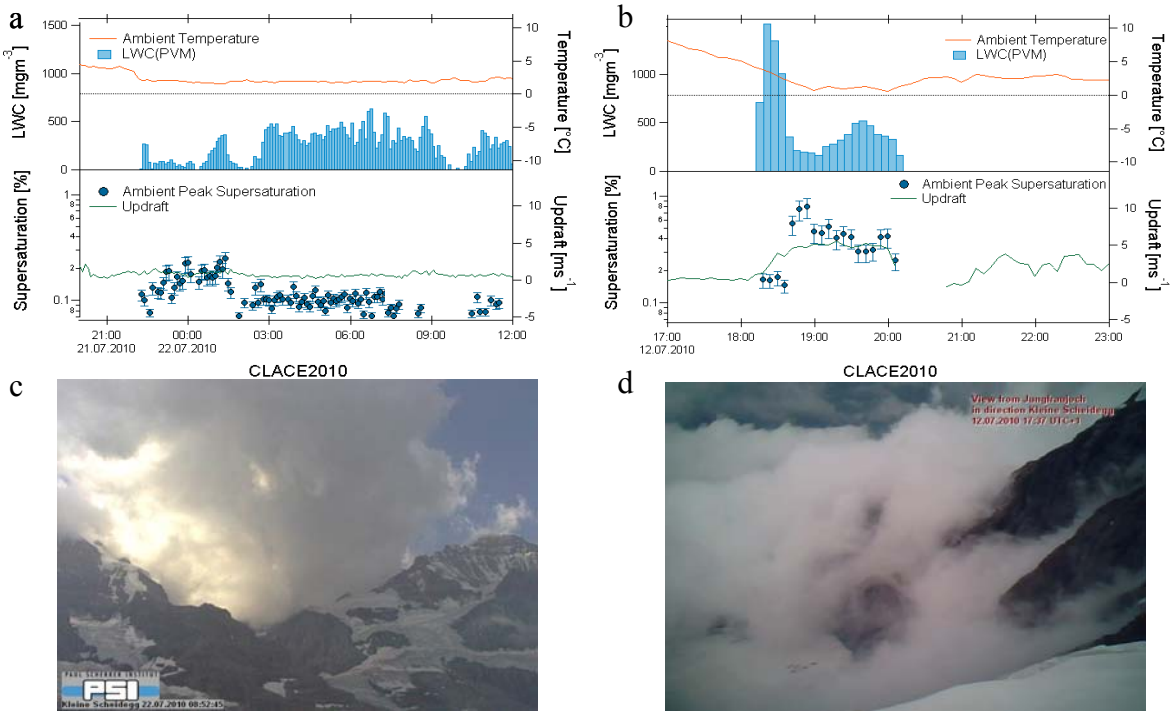

Fig. 4.17: An example for an advection and a convection cloud. (a) Advection cloud with low updraft velocities and quite constant SS_p. (b) Convection cloud with a rapid decrease in air temperature and a corresponding increase in supersaturation while updraft increases. The lower panel shows corresponding pictures taken by webcams from Kleine Scheidegg (c) and Jungfraujoch (d).

While air coming from the north, it can be seen that a slight increase in SS_p relates to larger w. Thus, the expected relationship between w and SS_p was found during convective cloud periods. However, the weak correlation (R^2=0.31) could be either an artifact of the air temperature measurement at the Kleine Scheidegg due to exposure to heat radiation at the ground, or due to too few measurements for measuring the lapse rate over this distance. Also the local measurement of w at the Jungfraujoch which does not allow to measure updraft velocities at the actual cloud formation, could bias the correlation. Another problem for this analysis was the frozen sonic anemometer during periods of high SS_p values. Since high SS_p lead to dense clouds more supercooled droplets were available and could freeze onto the sonic anemometer. To get supercooled droplets, w should be more than about 6 m s^{-1}. It has been observed that almost no data is available during cloud periods with air temperature below -8°C but w was slightly increasing up to this temperature (not shown). Hence, it is expected that during periods of a frozen sonic anemometer (no data available), w should have been quite high.

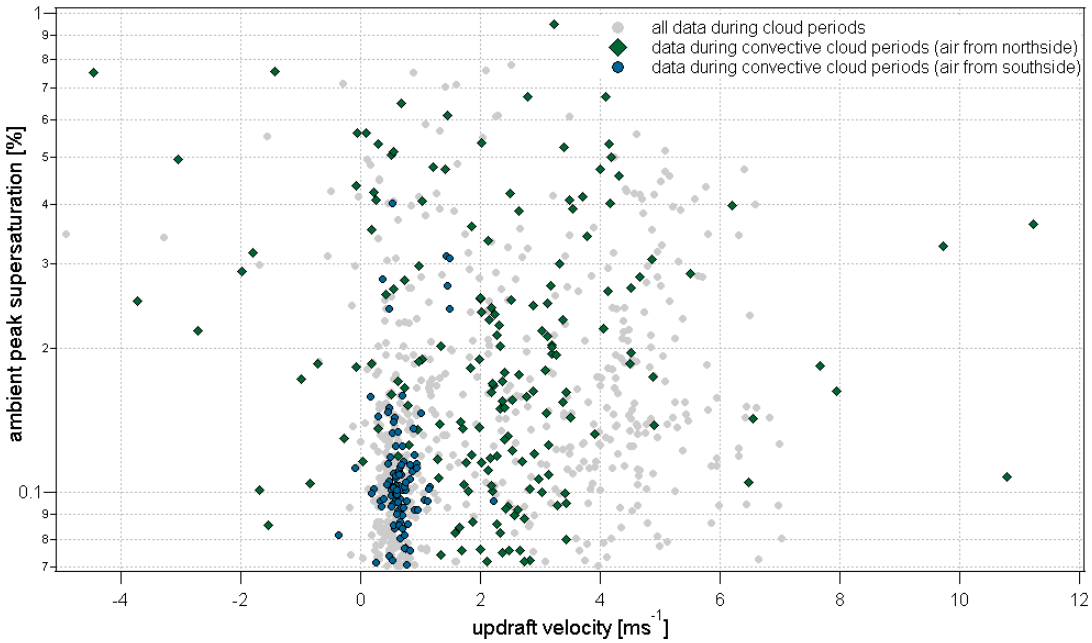

Fig. 4.18: Calculated ambient peak supersaturation versus updraft velocities has been plotted. Grey dots depict every data during stable cloud periods (30th percentile of LWC higher than 5 mg m^{-3}). Data during stable convective cloud periods (lapse rate < -0.7 K/100m) when air came from south (130 to 230°) are indicated with blue dots and from north (270 to 90°) with green diamonds.

5. Conclusion and Outlook

Cloud droplet size distributions were measured at the high-alpine site Jungfraujoch during a 9-week measurement campaign called CLACE2010 (Cloud and Aerosol Characterization Experiments). These measurements were conducted outside with a fog monitor (FM). Additionally, aerosol size distributions of total and interstitial aerosol were measured by two SMPS systems, respectively. During cloudless periods identical values of total number concentration of aerosols were measured for the different inlet types. When clouds were present, a weak agreement was found between CCN concentrations derived from the SMPS and cloud droplet concentrations measured by the FM. This unexpected issue was a result of freezing of the inlet and optical windows of the FM which thus led to interruptions of the flow of cloud droplets through the inlet. Hence, it can be concluded that the FM is a non-adaptable device at high-alpine sites where harsh weather conditions are present even during summer. For further campaigns, an ice selective inlet (equipped with optical particle counters) or an FSSP-100 instead of a FM could lead to better results. During summer 2000, a FSSP-100 was already being used at Jungfraujoch to measure cloud droplet size distributions. Results have shown quite a good agreement between CCN number concentrations derived from SMPS data and those measured by the FSSP (HENNING, 2002).

The application of the Clausius-Clapeyron theory to measurements of a Dew Point Hygrometer (DPH) has been found to be an adequate method for retrieving LWC. It could be shown that a DPH installed in the laboratory at Jungfraujoch connected to total inlet shows quite good results in comparison to the PVM. In contrast to the PVM, the DPH is not exposed to freezing processes. Therefore, measurements of LWC during summertime, when no ice particles are expected within clouds, could be carried out only using a DPH. In further campaigns, the difference between LWC data inferred from DPH measurements and measured by the PVM could be compared during wintertime. This would improve our knowledge about the ice content within a cloud during this season.

From the measured aerosol and cloud droplet size distributions the activation diameter (D_{50}) has been calculated over the whole time range of the campaign. The D_{50} was found to be influenced by LWC and the number concentration of cloud droplets below a certain LWC threshold. During CLACE2010 the threshold was observed at a LWC of 150 mg m^{-3}. Above this value D_{50} seems to depend on other parameters such as air temperature. It was found that above the freezing point D_{50} strongly increases with increasing air temperature. Furthermore, ambient peak supersaturation (SS_p) was calculated with a 17-month climatology of CCN number concentrations at 10 different supersaturations measured by a CCNC (JURÁNYI ET AL., 2011 in press). It has been found that supersaturations at Jungfraujoch have a mean value of 0.26% and a median value of 0.17%. These values are in quite good agreement with results from earlier studies where laboratory measurements have been applied to ambient conditions (HENNING, 2002; JURÁNYI ET AL., 2011 in press). Considering origin of air parcels it has been found that air coming from south most often result in SS_p values of ~0.1%. Air parcels coming from the north show a wider range of calculated SS_p values.

Since calculated standard deviations of the SS_p values retrieved from the 25th and 75th percentiles of the 17-month climatology of D_{50} are not that high, it can be concluded that for the calculation of SS_p values D_{50} is not the major component. Thus, it seems that D_{50} does not need to be measured highly correctly to retrieve valid SS_p values. It was observed that a decrease in air temperature correlated with an increasing SS_p. Furthermore, in some cases the updraft velocity relates to SS_p as well, but this issue needs to be further investigated. When distinguishing between convective and advective clouds it was observed that the former type corresponds well to increases in updraft velocity and SS_p. With data from the Windprofiler

and the Lidar the separation between these two cloud types may improve. Further, knowledge on the location of the activation of aerosols could be gained with these devices. It is expected that aerosol in convective clouds activated just before reaching Jungfraujoch but aerosols within advection clouds can activate above Kleine Scheidegg or even earlier.

Furthermore, a cloud model for the high-alpine site Jungfraujoch could be established with following parameters: T_{air}, updraft velocity and *PSA* which seems to be depending on SS_p. In order to evaluate this dependence an improved temperature profile must be available to assign a more adequate convective cloud period criterion. Also, a better size resolution of the data for advection clouds should be obtained.

References

Albrecht, B., 1989: Aerosols, cloud microphysics and fractional cloudiness. *Science*, **245**, 1227–1230.

Andrews, David G. 2010. *An Introduction to Atmospheric Physics 2nd Edition*. University of Oxford. Cambridge University Press.

Baltensperger, U., M. Schwikowski, D. T. Jost, S. Nyeki, H. W. Gäggeler, and O. Poulida, Scavenging of atmospheric constituents in mixed phase clouds at the high-alpine site Jungfraujoch, part 1, Basic concept and aerosol scavenging by clouds, *Atmos. Environ.*, **32**, 3975– 3983, 1998.

Chýlek, P., G. B. Lesins, G. Videen, J. G. D. Wong, R. G. Pinnick, D. Ngo, and J. D. Klett(1996), Black carbon and absorption of solar radiation by clouds, *J. Geophys. Res.*, 101(D18), **23**,365–23,371, doi:10.1029/96JD01901.

Corrigan, C. E., T. Novakov, Cloud condensation nucleus activity of organic compounds: a laboratory study, *Atmospheric Environment*, Volume 33, Issue 17, August 1999, Pages 2661-2668, ISSN 1352-2310, DOI: 10.1016/S1352-2310(98)00310-0.

Cozic, Julie, 2007: Aerosol properties of the free troposphere and their interference with mixed-phase clouds. PhD thesis. University of Bern

DMT, Fog Particle Spectrometer (fog monitor) Operations Manual, SPP-FM Electronics; 1999

Eugster, W., Burkard, R., Klemm, O., Wrzesinsky, T., 2001. Fog deposition measurements with the eddy covariance method. In: Schemenauer, R., Puxbaum, H. (Eds.), Proceedings of the Second International Conference on Fog and Fog Collection, St. John's, Canada, 15– 20 July 2001, pp. 193– 196.

Gerber H., 1991. Direct measurement of suspended particulate volume concentration and farinfrared extinction coefficient with a laser-diffraction instrument. *Appl. Opt.*, **30**, 4824−4831.

Gerber, H., 1998. Standards for Measuring Fog Liquid Water Content. In: R.S. Schemenauer and H. Bridgman (Eds.), *Proceedings of the 1st International Conference on Fog and Fog Collection*, Vancouver, Canada, ISBN 0-9683887-0-1, North York, Ontario, Canada, 149−152.

Hansen, J.E., and L.D. Travis, 1974: Light scattering in planetary atmospheres. *Space Sci. Rev.*, **16**, 527-610, doi:10.1007/BF00168069.

Hartz, Kara E. Huff, Joshua E. Tischuk, Man Nin Chan, Chak K. Chan, Neil M. Donahue, Spyros N. Pandis, Cloud condensation nuclei activation of limited solubility organic aerosol, *Atmos. Environ.*, **40**, 605-617, 2006.

Henning, S. (2002), Aerosol Chemistry and Cloud Interaction at the High-Alpine Site Jungfraujoch (3580masl), PhD thesis.

Henning, S., Weingartner, E., Schmidt, S., Wendisch, M., Gaggeler, H. W., and Baltensperger, U.: Size-dependent aerosol activation at the high-alpine site Jungfraujoch (3580 m asl), *Tellus B*, **54**, 82–95, 2002.

Houze, R. A., *Cloud Dynamics*, Academic, San Diego, Calif., 1993.

Intergovernmental Panel on Climate Change (IPCC) (2007), Climate Change 2007: The Physical Science Basis. Contribution of Working Group I to the Fourth Assessment Report of the Intergovernmental Panel on Climate Change, edited by S. Solomon et al., Cambridge Univ. Press, Cambridge, U. K., available at http://ipcc-wg1.ucar.edu/wg1/wg1-report.html.

Jensen, William B., The Universal gas constant R. Department of Chemistry, University of Cincinnati, Cincinnati, OH 45221-0172 *J. Chem. Educ.*, 2003, 80 (7), p 731 **DOI:** 10.1021/ed080p731

Jurányi, Zsofia, 2010: Characterisation of the cloud condensation nuclei properties of complex aerosols: from the smogchamber to the free troposphere. PhD thesis. Diss. ETH No. 19238.

Jurányi, Z., M. Gysel, E. Weingartner, N. Bukowiecki, L. Kammermann, and U. Baltensperger, 17-month climatology of the cloud condensation nuclei number concentration at the high alpine site Jungfraujoch, *Geophys. Res.*, 2011.

Jurányi, Z., Gysel, M., Weingartner, E., DeCarlo, P. F., Kammermann, L., and Baltensperger, U.: Measured and modelled cloud condensation nuclei concentration at the high alpine site Jungfraujoch, *Atmos. Chem. Phys.*, 2010.

Kammermann, L., Gysel, M., Weingartner, E., and Baltensperger, U.: 13-month climatology ofthe aerosol hygroscopicity at the free tropospheric site Jungfraujoch (3580 m a.s.l.), *Atmos. Chem. Phys.*, 10, 13573–13608, 2010.

Kammermann, Lukas, 2010: Aerosol hygroscopicity and CCN properties at remote sites. PhD thesis. Diss. ETH No. 18910.

Latham John, Philip Rasch, Chih-Chieh Chen, Laura Kettles, Alan Gadian,Andrew Gettelman, Hugh Morrison, Keith Bower, and Tom Choularton; Global temperature stabilization via controlled albedo enhancement of low-level maritime clouds, *Phil. Trans. R. Soc.*, 3969-3987, 2008.

Lowe, P. R.; J.M. Ficke, The computation of saturation vapor pressure. Tech.Paper No. 4-74 Environmental Prediction Research Facility, Naval Postgraduate School, Monterey, CA., 1974

McFiggans, G., Artaxo, P., Baltensperger, U., Coe, H., Facchini, M. C. and co-authors. 2006. The effect of physical and chemical aerosol properties on warm cloud droplet activation. *Atmos. Chem. Phys*. 6, 2593–2649.

Nenes, A., Chuang, P. Y., Flagan, R. C., and Seinfeld, J. H.: A theoretical analysis of cloud condensation nucleus (CCN) instruments, *J. Geophys. Res.*-A., **106**, 3449–3474, 2001.

Nessler, Remo, Dry and Ambient Aerosol Properties at the Jungfraujoch. PhD thesis. University of Bern

Penner, J.E., et al., 2001: Aerosols, their direct and indirect effects. In: Climate Change 2001: The Scientifi c Basis. Contribution of Working Group I to the Third Assessment Report of the Intergovernmental Panel on Climate Change [Houghton, J.T., et al. (eds.)]. Cambridge University Press, Cambridge, United Kingdom and New York, NY, USA, pp. 289–348.

Prenni, A. J., M. D. Petters, S. M. Kreidenweis, P. J. DeMott, and P. J. Ziemann (2007), Cloud droplet activation of secondary organic aerosol, *J. Geophys. Res.*, **112**, D10223, doi:10.1029/2006JD007963.

Raoult, F.-M. General law of the vapor pressure of solvents. *Comptes Rendus* **1887**, *104*, 1430−3.

Roberts, G. C. & Nenes, A. (2005). A Continuous-Flow Streamwise Thermal-Gradient CCN Chamber for Atmospheric Measurements. *Aerosol Science and Technology*, *39*(3), 206-221. doi:10.1080/027868290913988

Rogers, R. R., 1975: An elementary parcel model with explicit condensation and supersaturation. *Atmosphere,* **13,** 192–204.

Schwikowski, M. H., Seibert, P., Baltensperger, U. and Gaggeler, H. W. (1995) A study of an outstanding Saharan dust event at the high-alpine site Jungfraujoch, Switzerland. *Atmospheric Environment* **29**, 1829-1842.

Seinfeld, John H. ; Pandis, Spyros N. Atmospheric Chemistry and Physics - From Air Pollution to Climate Change (2nd Edition). John Wiley & Sons. 2006.

Verheggen, B., J. Cozic, E. Weingartner, K. Bower, S. Mertes, P. Connolly, M. Gallagher, M. Flynn, T. Choularton, and U. Baltensperger (2007), Aerosol partitioning between the interstitial and the condensed phase in mixed-phase clouds, *J. Geophys. Res.*, 112, D23202, doi:10.1029/2007JD008714.

Wallace, J. and P.V. Hobbs. 2006. Atmospheric Science: An Introduction Survey. Elsevier Science and Technology Books

Weingartner, E., S. Nyeki, and U. Baltensperger (1999), Seasonal and diurnal variation of aerosol size distributions (10 < D < 750 nm) at a high-alpine site (Jungfraujoch 3580 m asl), *J. Geophys. Res.*, **104**(D21), 26,809–26,820, doi:10.1029/1999JD900170.

WMO (2003), WMO/GAW Aerosol Measurement Procedures Guidelines and Recommendations, (WMO TD No. 1178) – GAW Report No. 153, World Meteorological Organization, http://wdca.jrc.it/data/gaw153.pdf, Geneva.

A. Background information about fog monitor

A.1. True Air Speed of fog monitor

The total number concentration of cloud droplets depends on the true air speed (TAS) of fog monitor – this can be seen in Equation A.1. Fig. A.1 shows the time series of the TAS during the whole measurement campaign, while the different colors depict the ambient temperature measured by MeteoSwiss. It can be seen that the TAS data is very noisy. Thus, it is difficult to calculate the total number concentration without having a further look at the TAS.

$$N_{tot} = \frac{\sum_{i=0}^{m} N_i}{A \cdot t \cdot v_{flow}}$$

A: effective beam diameter
v_{flow}: TAS of Fog Monitor
t: Sampling time
N_i: Counts of droplets in bin i

Equation A.1

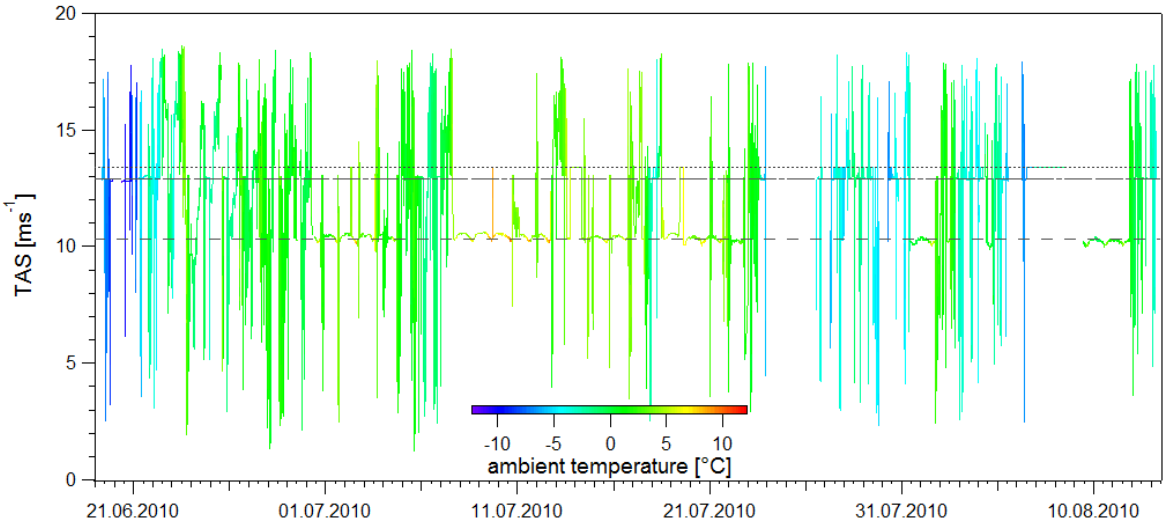

Fig. A.1: Time series of TAS from fog monitor as function of ambient temperature depicted in different colors. Three lines show levels of assembling points. Uppermost line (dots) shows level of substituted outliers with a value of 13.41 ms^{-1}. Middle line (long dashes) shows level of TAS during rather cold periods and lowermost line (short dashes) shows values measured during rather warm periods.

Bug detection

The three different lines show levels where most of the points are assembled in three different classes. The upper line with dots depicts values that are written automatically if an outlier is available. It is on the level of 13.41 ms^{-1}. The second upper line with long dashes shows a level of TAS most often seen in blue or lime green colors and consequently means during cold periods. The line is at a level of 12.8 ms^{-1}. The lowermost dashed line represents most of the data points at the level of 10.3 ms^{-1}. Due to the strong noise it is not appropriate to calculate a mean value and use it to determine the total number concentration of droplets. A further analysis has been done by calculating temperature classes for the different TAS. Fig. A.2 shows the three quartiles, and the 10^{th} and 90^{th} percentile of TAS separated to six temperature classes.

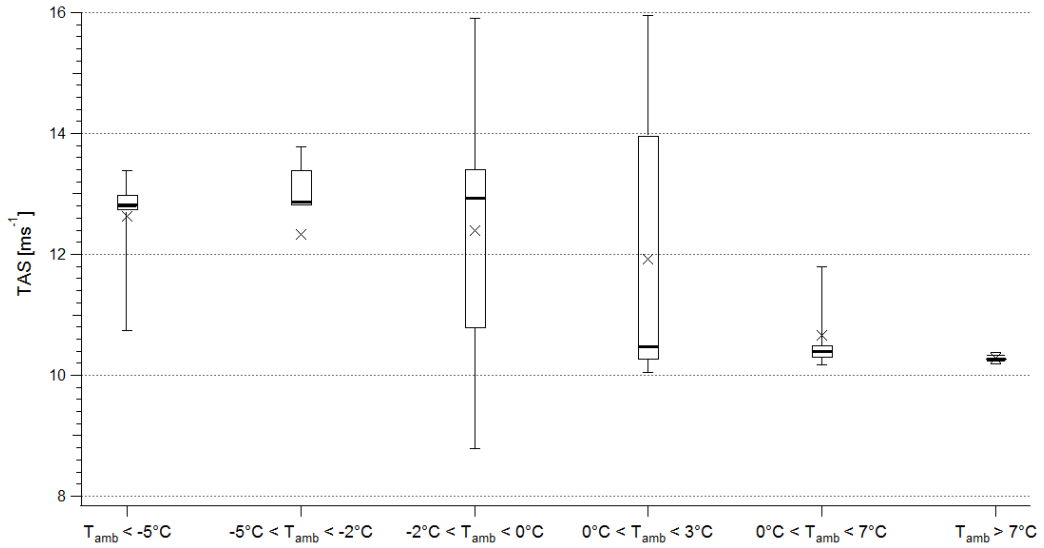

Fig. A.2: TAS of FM (10th, 25th, median, 75th and 90th percentile) plotted versus ambient temperature in six different classes. Only values where absolute wind speed was below 0.5 ms^{-1} were used for calculations.

Only data where the absolute wind speed v_{abs} $\left(v_{abs}(u,w,z)=\sqrt{u^2+v^2+w^2}\right)$ was below 0.5 ms^{-1} has been considered to neglect disturbances arising from wind directions not directed into the inlet of the FM. It can be clearly seen that the median of TAS is quite constant at a level of 12.8 ms^{-1} for temperatures below 0°C, and above the freezing point it is quite constant at a level of 10.3 ms^{-1}. Thus, TAS does not linearly increase with temperature; there must be a threshold at 0°C. To avoid the noise and to be sure using the correct level, the value 10.3 ms^{-1} will be used for ambient temperatures above 0°C and 12.8 ms^{-1} for temperatures below 0°C.

Considering source code of data handling software from Werner Eugster the issue of two different levels of TAS can be explained as follow: If measured static pressure is not within range of 800 and 1100 hPa it was set to 916 hPa. At the Jungfraujoch air pressure during CLACE2010 campaign was around 660 hPa (see Figure 4.1). Thus, there was only a variation in dynamic pressure and led to a too low TAS value of about 10.3 ms^{-1}. When FM was frozen dynamic pressure was below 0 hPa and a standard value of 0.97 hPa has been set. This led to the value of 12.8 ms^{-1}. After debugging, a mean TAS value of 13 ms^{-1} has been taken for the analysis of data from CLACE2010 campaign.

Diurnal variation

Zooming in Fig. A.2 another interesting aspect can be seen. During periods without strong noise, a clear daily variation of TAS from FM can be seen in Fig. A.3. Applying the knowledge from results above, it can be concluded that the daily variation is due to the daily fluctuations of ambient temperature. During this campaign a strong variation of ambient temperature was present due to very warm conditions at the Jungfraujoch during day, especially during the month of July.

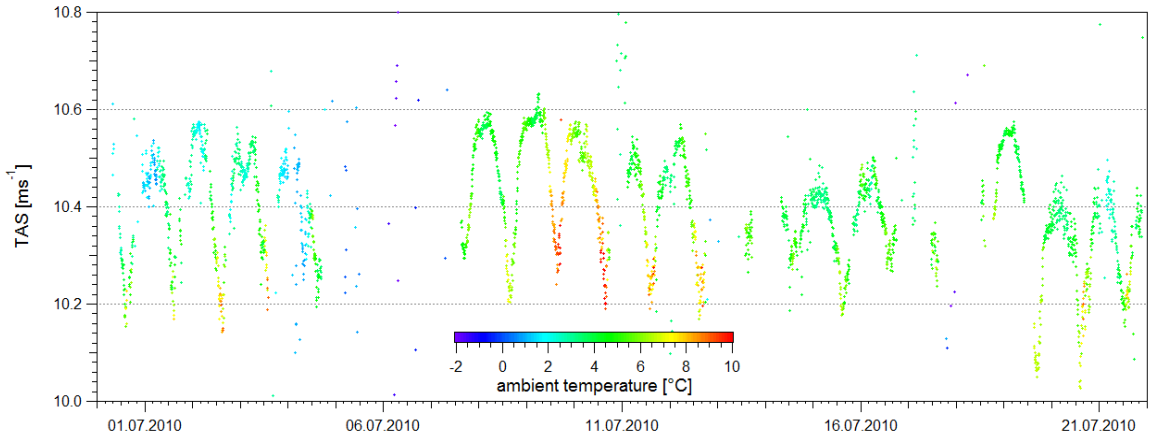

Fig. A.3: Daily variation of TAS of fog monitor depicted as function of ambient temperature in different colors. Time period has been randomly chosen for a period where the noise was quite small.

A.2. Size bin classification

FM has to be calibrated with glass beads to classify cloud droplets to size classes later on. There were six different sizes of glass beads which determine the 40 size bins. With a conversion equation from Mie theory the different bins for cloud droplets can be calculated. For glass beads a calibration size of n=1.51 and for water n=1.33 have been used. After applying this calibration and conversion table from DMT (Droplet Measurement Technologies, Boulder CO) following bin sizes for cloud droplets have been retrieved:

1.5000, 1.7032, 2.2754, 3.7696, 5.9306, 7.8134, 9.2456, 10.3900, 11.4153, 12.2211, 12.8871, 13.7391, 14.9590, 16.2825, 17.5717, 18.9114, 20.2244, 21.4517, 22.6837, 23.9506, 25.1593, 26.3140, 27.4567, 28.5995, 29.6984, 30.7773, 31.9509, 33.1694, 34.3748, 35.5826, 36.7896, 38.0087, 39.2488, 40.5227, 41.8443, 43.2075, 44.5863, 45.9188, 47.2079, 48.5633, 50.0000 µm

B. CCNC measuring problem

During CLACE2010 campaign cloud condensation nuclei counter (CCNC) measured too high CCN concentrations over certain periods. Lower panel of Fig. B.1 shows measured CCN concentrations for the different supersaturations (different colors) and the total number concentration of aerosols measured by an SMPS. It can be clearly seen that number concentration of CCN measured by CCNC is sometimes larger than number concentration of aerosols. This impossible issue could not be verified with a leak in air flow (see Fig. B.1, upper panel) since post-measured sample flow in laboratory showed lower values than calibration constants used during CLACE2010 campaign. Anyway, smaller measured sample flow values than calibrations values set would lead to smaller concentrations and thus resolve in wrong direction (see Fig. B.2). Measured sheath flow show same values than used calibration values during CLACE2010 campaign so that this flow cannot be a problem.

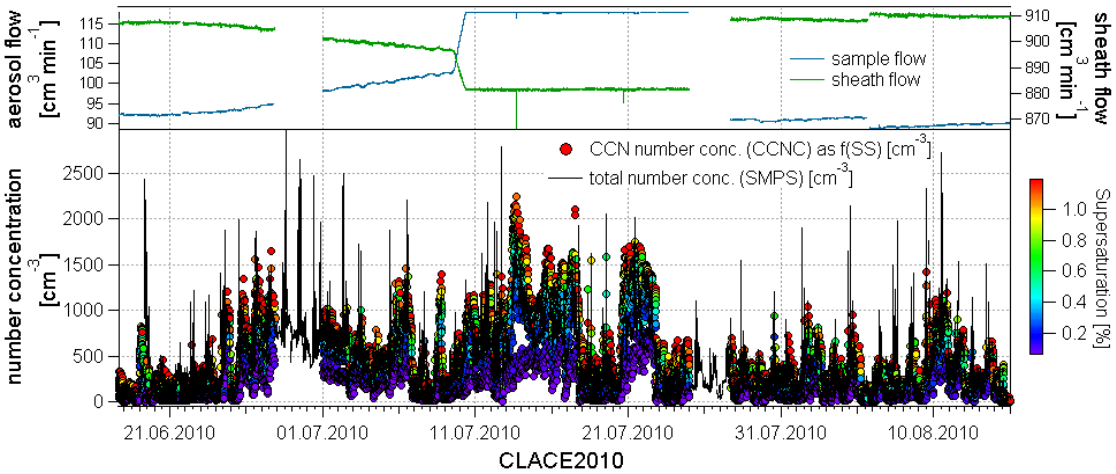

Fig. B.1: Calculated sheath and sample flow values from CCNC during CLACE2010 (upper panel). On 10 July, an unknown decrease of sheath to sample flow ratio occurred. On 28 July, the low sheath to sample flow ratio has been detected and regulated. On 5 August, a power interruption at the Jungfraujoch occurred. Lower panel: Total number concentration measured by SMPS (black line) and CCN number concentration measured by CCNC for different supersaturations over whole CLACE2010 campaign is plotted.

Sheath to sample flow ratio show a slight decrease since beginning of CLACE2010 campaign. On 10 July sheath to sample flow ratio strongly decreased for reasons which are not clear. On 28 July this decrease in flow ratio has been detected and regulated. The slight increase in flow ratio on 5 August was due to a power interruption at the Jungfraujoch.

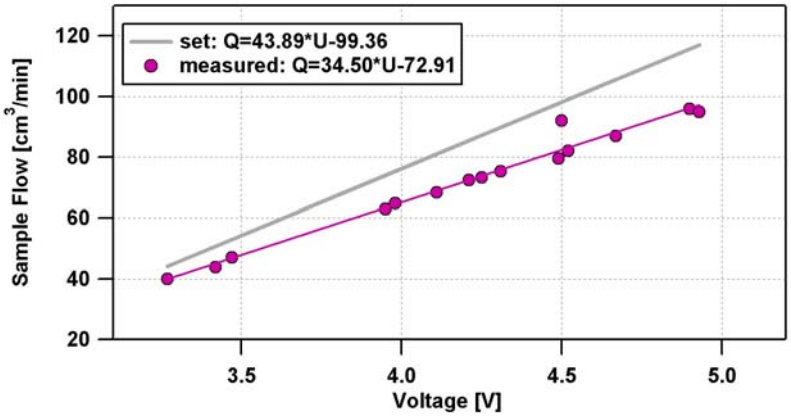

Fig. B.2: Calculated sample flow of CCNC during CLACE2010 (grey) and measured sample flow in laboratory at PSI (violet) are depicted.

Jurányi et al. (2011 in press) showed that D_{50} remain quite constant over whole year. Thus, number concentration of CCN for a certain supersaturation should be of same value as integrated size distribution of SMPS with lower boundary of D_{50} retrieved for corresponding supersaturation. Fig. B.3 shows that measuring error of CCNC is for every supersaturation almost the same but vary over time. Hence, an adequate correction factor cannot be applied.

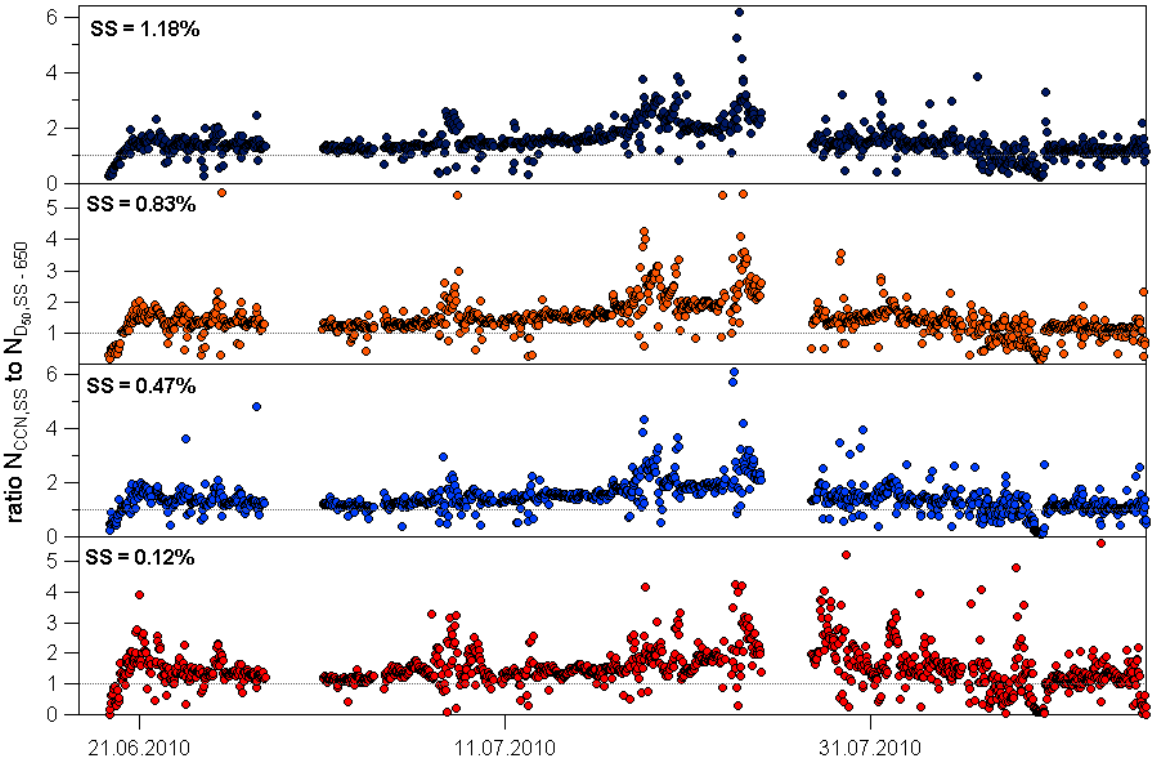

Fig. B.3: Ratio of CCN number concentration to number concentration of integrated SMPS size distribution with lower boundary of D50 from corresponding supersaturation. Ratios are shown for four examples of supersaturation.

List of Figures

List of Tables

Acknowledgements

During the work for my Master thesis at Paul Scherrer Institut (PSI), Laboratory for Atmospheric Chemistry (LAC) a lot of people helped me in different ways. This work involves a measurement campaign where a lot of people supported me and the two measurement devices I was responsible for. Thus, a lot of scientists but also non-scientists are involved in this work and to all them I like to thank.

- **Prof. Dr. Margit Schwikowski** was the starting shot for this thesis. She gave me the contact details for the PSI. I like to thank you for being my advisor and responsible person from University of Berne.

- **Prof. Dr. Urs Baltensperger** made it possible that I could write my thesis at PSI. I like to thank you for being my Supervisor and that I could spend a nice time at LAC.

- **Dr. Ernest Weingartner** was the head of my co-supervisors and supported me very well during my work. Whenever I had a question or a problem with some scientific stuff, you had an open door – even when you were busy. I like to thank you for all that and also for the motivation you gave me whenever I ground to a halt.

- **Dr. Nicolas Bukowiecki** was the first person I saw at my first day at PSI. He showed me all the buildings, my office and introduced me to the LAC. I like to thank you for being such a good co-supervisor! At the Jungfraujoch you looked very well at the measurement devices I was responsible for and always informed me when something went wrong. You had always an open door for every question I had. Thank you for all the time you supported me!

- **Dr. Zsófia Jurányi** was my teacher in IGOR and physics. Whenever I had problems with IGOR you helped me. You brought me to a level where I can say: 'I like IGOR'. I like to thank you for all the time you took to introduce me e.g. in working principles of measurement devices but also in showing me the different tunnels at the Jungfraujoch together with Nicolas.

- **Dr. Martin Gysel** was the person who saw always a way out of every scientific problem I had. Thank you for supporting me during my thesis!

- **PD. Dr. Werner Eugster & Johanna Spiegel** were the persons who provided a sonic anemometer for the CLACE2010 campaign since the device from PSI broke down few months before the campaign should start. You taught me how to cope with Linux and using your software. Whenever I struggled with the FM you had an open door. During the CLACE2010 campaign you helped me installing the two devices, although, Werner was far away in Alaska. Thank you for all your support!

- **Paul Zieger** was the one who went out of the Sphinx building to de-ice the FM and the sonic anemometer, hour by hour, only for delivering me good data. I think to yoke me to the sledge to drive you to the Monchsjochhütte was fair enough. Thank you for all your help and nice time at the Jungfraujoch!

- **Günther Wehrle, René Richter & Bettina Möhrle** were the persons who supported me with computers, hard disks, fixing material and installation help. Rene, thank you for creating a fixation for the sonic anemometer. Thank you for all your work and support!

- **Custodians at the Jungfraujoch (HFSJG)** were the persons who looked that I had always a clean room and a nice stay at the Jungfraujoch. Thank you!

- **Sophie-Berenice Wilmes** helped me improving my English within my Master's thesis. I like to thank you for taking the time to help me with some translations and corrections.

- A big thank goes to **my family**! Thank you that you gave me the opportunity to study and supporting me during this time!

Declaration

under Art. 28 Para. 2 RSL 05

Last, first name: Hammer, Emanuel.....

Matriculation number: 05-053-707.....

Programme: Climate Sciences…….....

Bachelor ☐ Master ☒ Dissertation ☐

Thesis title: Calculation and interpretation of cloud peak supersaturations at the Jungfraujoch

Thesis supervisors: Prof. Dr. Urs Baltensperger, Prof. Dr. Margit Schwikowski, Dr. Ernest Weingartner, Dr. Nicolas Bukowiecki, Dr. Zsófia Jurányi & Dr. Martin Gysel

I hereby declare that this submission is my own work and that, to the best of my knowledge and belief, it contains no material previously published or written by another person, except where due acknowledgement has been made in the text. In accordance with academic rules and ethical conduct, I have fully cited and referenced all material and results that are not original to this work. I am well aware of the fact that, on the basis of Article 36 Paragraph 1 Letter o of the University Law of 5 September 1996, the Senate is entitled to deny the title awarded on the basis of this work if proven otherwise.

Villigen, 03/02/2011

Place, date

.....

Signature